Deglaciation and postglacial evolution of the Cère Valley (Cantal, French Massif Central) based on geomorphological mapping, 36 Cl surface exposure dating and glacier modelling

Arthur Ancrenaz, Stéphane Pochat, Vincent Rinterknecht, Laura Rodríguez-rodríguez, Emmanuelle Defive, Alexandre Poiraud, Vincent Jomelli, Irene Schimmelpfennig, Aster Team

Deglaciation and postglacial evolution of the Cère Valley (Cantal, French Massif Central) based on geomorphological mapping, ^{36}Cl surface exposure dating and glacier modelling

ARTHUR ANCRENAZ,[1]* STÉPHANE POCHAT,[2] VINCENT RINTERKNECHT,[3] LAURA RODRÍGUEZ-RODRÍGUEZ,[4] EMMANUELLE DEFIVE,[1] ALEXANDRE POIRAUD,[1] VINCENT JOMELLI,[3] IRENE SCHIMMELPFENNIG[3] and ASTER TEAM[3†]

[1]Université Clermont Auvergne, CNRS, GEOLAB, F-63000, Clermont-Ferrand, France
[2]Laboratoire de Planétologie et Géosciences, LPG, UMR 6112, Nantes Université, CNRS, France
[3]Aix Marseille Univ, CNRS, IRD, INRAE, CEREGE, BP 80, 13545, Aix-en-Provence Cedex 4, France
[4]Departamento de Geología, Universidad de Oviedo, c/Jesús Arias de Velasco s/n, 33005, Oviedo, Spain

ABSTRACT: The landform assemblage in the Cère Valley (Cantal, France) provides one of the most complete sequences for Late Pleistocene glacial fluctuations in the French Massif Central. However, the associated glacial chronology has been debated since the 1980s. This paper aims to improve the glacial chronology of the Cère Valley using ^{36}Cl surface exposure ages. Geomorphological results define two glacier stadials with reconstructed equilibrium line altitudes of 1078 ± 43 and 1152 ± 34 m above sea level. These results are comparable to those obtained in the Alps or the Pyrenees during the Last Glacial Maximum (26–19.5 ka). However, ^{36}Cl surface exposure ages are centred around the Younger Dryas (YD), between 13 and 11 ka (n = 4). We suggest that these ^{36}Cl ages are not related to a standstill during the YD but rather to the effects of the postglacial evolution of the Cère Valley. We investigate two geomorphological end-member scenarios to explain the postponed exposure of sampled boulders: the Aurillac Lake scenario and the later fluvial incision scenario. While the nature of the geomorphological events leading to the boulder exhumation is not fully resolved, we highlight a long phase of postglacial evolution in the Cère Valley.

KEYWORDS: ^{36}Cl surface exposure dating; Cantal; glacial geomorphology; Late Pleistocene; palaeoclimate

Introduction

At present, the glacial history of the Cantal-Cézallier-Monts Dore (CCMD) in the French Massif Central is poorly known despite early observations of past glacial imprints (Boule, 1896, 1895; Glangeaud, 1921; Julien and Laval, 1868; Rames, 1873) that led to numerous geomorphological studies (Boisse de Black, 1951; Goër de Hervé, 1972; Valadas, 1984; Van Dorsser, 1986, 1982; Veyret, 1978). This is especially true when it comes to the last glacial extents and timing for which large uncertainties remain (Define *et al.*, 2019; Etlicher and Goër de Hervé, 1988). The geomorphological reconstructions of the CCMD glacier system were based on a sequence of end moraines located in the main Cantal valleys (Cère, Authre, Jordanne, Alagnon, Rhue) and Monts Dore valleys (Dordogne, Tarentaine) (Boisse de Black, 1951; Goër de Hervé, 1972; Valadas, 1984; Veyret, 1978). Most of the glacial remnants were associated with the last glaciation and are used to define three glacial stadials. The oldest, inferred to the Local Last Glacial Maximum (LLGM), was defined by the outermost end moraines or till deposits. A younger glacier re-advance, locally named the Recurrence Event, was defined by end moraines located upstream of the LLGM deposits. The end of the Recurrence Event started with the lowland deglaciation, i.e. Artense plateau and lower parts of valleys and plateaus of the CCMD. A final cirque glacier stadial was represented by end moraines located in two main Cantal head valleys: the Impradine and Lagnon valleys (Valadas, 1984). In addition, isolated patches of till were interpreted as pre-LLGM deposits and were associated with Middle-Pleistocene glaciations based on their location downstream of the LLGM deposits and their more intense weathered aspect (Goër de Hervé, 1972; Van Dorsser, 1982; Veyret, 1978).

The existing chronologies of the deglaciation sequence were constrained by indirect palaeoenvironmental data. The timing of the LLGM was correlated with the timing of the glacier maximum extent in the Alps (Veyret, 1978), which is attributed to the global Last Glacial Maximum (LGM) (27.5–23.3 ka *sensu* Hughes and Gibbard, 2015). The timing of the last deglaciation in the Cantal Mounts is constrained by a single radiocarbon age (Veyret-Mekdjian *et al.*, 1978) obtained from the Lugarde kame terrace in the Santoire Valley at 900 m above sea level (a.s.l.) (north of Cantal; Fig. 1 for the location). This kame deposit includes a layer rich in organic matter dated from 17.1 to 15.7 ka cal BP (2 sigma radiocarbon age calibrated with the CLAM v.2.3.2 software and the 'IntCal20' calibration curve; Blaauw, 2010; Reimer *et al.*, 2020) that was buried by a till deposit associated with a glacier advance. In addition, indirect chronological boundaries for deglaciation steps were provided by a pollen stratigraphy established in the CCMD deglaciated slopes. The typical Oldest Dryas (18.5–15.3 ka *sensu* Degeai and Pastre, 2009) pollinic assemblage defined at the Lake Bouchet at 1250 m a.s.l. (Fig. 1 for location) is *Artemisia* optimum with increasing *Juniperus* and *Betula* (Reille and Beaulieu, 1988). This assemblage was reported in the CCMD deglaciated slopes but not directly dated: (i) on the Artense plateau between ~400 and ~1000 m a.s.l. (Vergne, 1991); (ii) on the northern flank of the Cantal at the Taphanel

*Correspondence: Arthur Ancrenaz, as above.
Email: arthur.ancrenaz@doctorant.uca.fr
†ASTER Team: Georges Aumaître, D. Bourlès, K. Keddadouche

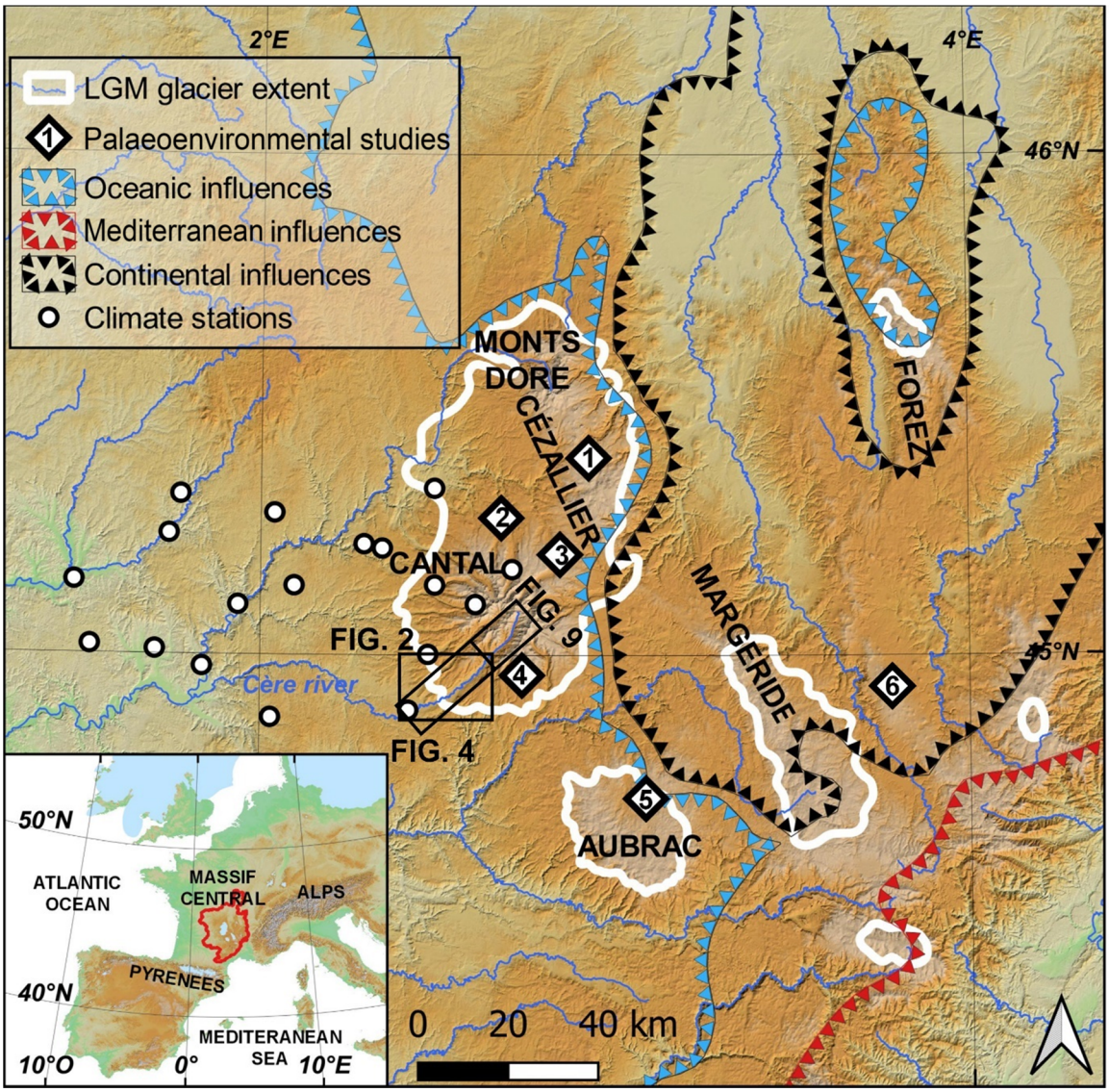

Figure 1. Location map of the Cère Valley in the Cantal–Cézallier–Mont Dores glacial system (CCMD), with Local Last Glacial Maximum (LLGM) extent in the Massif Central (Ehlers *et al.*, 2011), and main actual atmospheric influences. Numbers correspond to localities cited in the main text: (1) Godivelle, (2) Lugarde kame terrace from where the ^{14}C age was obtained, (3) Taphanel, (4) Peyre, (5) Roustières, (6) Lake Bouchet. [Color figure can be viewed at wileyonlinelibrary.com]

site, 975 m a.s.l. (Ponel *et al.*, 1991; Ponel and Russell Coope, 1990); and (iii) on the southern flank of the Cantal at the Peyre site, 1100 m a.s.l. (Miras *et al.*, 2006) (Fig. 1 for the location). In the Aubrac Mounts, at the Roustières site (1195 m a.s.l.; Fig. 1), radiocarbon ages for this pollinic assemblage range between 17.7 and 15.0 ka cal BP (Gandouin *et al.*, 2016; Ponel *et al.*, 2016). According to these local palaeoenvironmental data, two different relative chronologies for deglaciation steps in the CCMD are still debated (Veyret, 1978; Etlicher and Goër de Hervé, 1988):

- After Veyret (1978), the Recurrence Event buried the Lugarde kame terrace during the Oldest Dryas. CCMD lowlands were deglaciated at the end of the Oldest Dryas and the beginning of the Bølling–Allerød (15.3–12.8 ka *sensu* Degeai and Pastre, 2009). Finally, the timing of the cirque glacier stadial was correlated with the Younger Dryas (YD) cold event, between 12.8 and 11.7 ka (*sensu* Degeai and Pastre, 2009).
- After Etlicher and Goër de Hervé (1988), the Recurrence Event was older than the Oldest Dryas. The till that buried the Lugarde kame terrace was associated with a minor glacier advance after the lowland deglaciation. This advance took place at the latest during the Oldest Dryas. The cirque glacier stadial was correlated with the Oldest Dryas or the Bølling–Allerød.

The latter relative chronology for the CCMD deglaciation steps (Etlicher and Goër de Hervé, 1988) is broadly supported by direct chronological constraints established in the neighbouring Aubrac Mounts by ^{10}Be and ^{26}Al exposure ages (Ancrenaz *et al.*, 2022). In this area, glacial fluctuations from the LLGM to the last glacial advance were reported by geomorphological mapping and were dated between 27 and 17 ka. The full deglaciation of the Aubrac was dated to ~17 ka, during the Oldest Dryas. These findings are comparable to findings obtained at a regional scale. For example, LGM glacier advances were identified in the Alps (Wirsig *et al.*, 2016 and references therein), in the Pyrenees (Calvet *et al.*, 2011; Reixach *et al.*, 2021) and on the Iberian Peninsula (Domínguez-Villar *et al.*, 2013). Glacier recessions started at ~19 ka in the Alps (Wirsig *et al.*, 2016) or ~20 ka in the Pyrenees (Delmas *et al.*, 2011) and the Oldest Dryas was recognised as a glacier recession period over the entire Mediterranean basin (Allard *et al.*, 2021).

The aim of this study is to update the existing indirect and relative chronology for the CCMD glaciation by revising the

morphostratigraphic framework in the Cère Valley (Cantal). We combined ^{36}Cl surface exposure dating and former glacier geometry modelling to reconstruct palaeo-equilibrium line altitudes (ELAs) and associated climatic conditions during the last deglaciation. We chose the Cère Valley (Cantal) because the most complete sequence of glacier fluctuations in the CCMD, and by extension in the Massif Central, has been preserved. Four main features were described: (i) the Tronquières moraine, a pre-LLGM glacial deposit; (ii) the Carnéjac terminal moraine and associated proglacial outwash that delimits the LLGM; (iii) the Polminhac recessional moraine delimiting the Recurrence Event; and (iv) the Vic-sur-Cère end moraine delimiting a glacier standstill during the deglaciation.

Study area

The Cère Valley is one of the deepest (350–150 m) and longest (30 km) radial valleys of the Cantal Mounts, a Mio-Pliocene stratovolcano. As other Cantal valleys, the Cère Valley was formed by the combined action of fluvial and glacial erosion in favourable volcano-tectonic settings (Valadas, 1984). The upper part of the valley, from the Col de Font de Cère at 1290 m a.s.l. to the Pas de la Cère (~700 m a.s.l.), developed into trachyandesite along 15 km (Leibrandt, 2011; Nehlig *et al.*, 2001). The lower part of the Cère Valley, from the Pas de la Cère to the Aurillac basin was incised into volcanic breccias, mainly debris avalanch or debris flow (Arnaud *et al.*, 2002), Oligo–Miocene sediments and Paleozoic basement. Valley slopes were affected by large landslides of various nature (mainly deep-seated gravitational slope deformation and rockfall) but of unknown age and favoured by geological and topographic settings (Valadas, 1984; Van Dorsser, 1982, 1986).

During the LLGM, the Cantal glacier was a radially drained icefield or icecap (2.5×10^3 km^2) with an accumulation zone centred over the northwestern part of the Cantal (Goër de Hervé, 1972; Veyret, 1978) (Fig. 1). Radial valleys, such as the Cère Valley, canalised glacier outlets from the central accumulation zone towards the margin. The orographic effect of the Cantal (west windward exposed slopes are much wetter than downwind exposed slopes) is responsible for the dissymmetric extent of valley glaciers (Veyret, 1978). The northwestern Cantal valleys were occupied by longer glaciers, up to 30 km, and the eastern valleys were occupied by shorter glaciers, up to 20 km (Fig. 1). To the north, the Cantal, the Cézallier and the Monts Dore glaciers were coalescent, forming the CCMD glacier system (Fig. 1). The Cère glacier extended from the Col de Fond de Cère to the Aurillac basin at ~600 m. The particularity of the lower part of the Cère Valley is related to its flat bottom, with infilling of Pleistocene fluvio-glacial sediments (Van Dorsser, 1982; Veyret, 1978) reaching up to 10–20 m thick (Fig. 2).

Methodology

Glacial features inventory

Our geomorphological mapping aims to decipher the distribution of Late Pleistocene glacial landforms and sediments, paying special attention to ice-marginal landforms that indicate the extents of former glaciers (Kleman and Borgström, 1996). Postglacial deposits, generated by slopes or fluvial processes, such as landslides, colluvial accumulation, alluvial fans or alluvial terraces were also mapped. The mapping was elaborated using: (i) the inventory of glacial features from the literature (Boisse de Black, 1951; Valadas, 1984; Van Dorsser, 1982; Veyret, 1978); (ii) aerial photography (25 cm resolution) and digital elevation models (DEMs; 1 m resolution from LIDAR) delivered by the Institut national de l'information géographique et forestière (IGN); and (iii) *in situ* (i.e. in the field) verification and description. Mapping was performed using geographical information system (GIS) software (ArcGis).

Surface exposure dating using ^{36}Cl

Sampling strategy

In the Cère Valley, six moraine boulders were identified as suitable objects for surface exposure dating (Fig. 3). One was located on the Cavanhac plateau (sample CTL-04), three on the Carnéjac end-moraine (samples CTL-01, -02, -03) and two on the Polminhac end-moraine (samples CTL-20, -21) (Figs. 2 and 3). Samples for ^{36}Cl dating were collected in the field from top flat surfaces (up to 5 cm thick) of volcanic boulders (basalt and volcanic breccias) using a hammer and a chisel. Sampling was performed on moraine boulders with a broad base embedded in the glacial landform to minimise potential post-depositional disturbance. Sample locations and elevations were recorded using a hand-held GPS with elevations cross-checked with the DEM. Skyline measurements were taken using a compass-clinometer and topographic shielding factors were calculated using the skyline calculator within the CRONUS online calculator (Balco *et al.*, 2008; http://stoneage.ice-d.org/math/skyline/skyline_in.html; accessed 14 September 2019). Sample information is reported in Table 1.

Sample preparation and age calculation

Samples were crushed and sieved to 250–500 μm at CEREGE (Aix-en-Provence, France). Chlorine was extracted and purified from whole-rock samples to produce AgCl for accelerator mass spectrometry (AMS) analysis, following the procedure described by Schimmelpfennig *et al.* (2011). About 2 g of the bulk rock and 2 g of the chemically treated sample fractions were sent to SARM (Nancy, France) for chemical composition analyses (Tables 2 and 3). ^{35}Cl/^{37}Cl and ^{36}Cl/^{35}Cl ratios were measured by AMS at the 5 MV accelerator ASTER at CEREGE (Arnold *et al.*, 2013). Use of an isotopically enriched carrier allows simultaneous determination of the ^{36}Cl and the natural Cl concentrations of the dissolved samples. For normalisation of the ^{36}Cl/^{35}Cl ratios, an in-house standard with a given ^{36}Cl/^{35}Cl value of $1.42 \pm 0.02 \times 10^{-12}$ was used (Merchel *et al.*, 2011). Blank corrections were performed by subtracting the number of atoms of ^{36}Cl and Cl in the blanks from those in the samples, respectively.

^{36}Cl ages were calculated with the Excel spreadsheet of Schimmelpfennig *et al.* (2009), using the time-invariant scaling method from Stone (2000) and employing the following ^{36}Cl production rates, referenced to sea level and high latitude: 42.2 ± 4.8 atoms ^{36}Cl (g Ca)$^{-1}$ yr^{-1} for spallation of Ca (Schimmelpfennig *et al.*, 2011), 148.1 ± 7.8 atoms ^{36}Cl (g K)$^{-1}$ yr^{-1} for spallation of K (Schimmelpfennig *et al.*, 2014), 13.0 ± 3.0 atoms ^{36}Cl (g Ti)$^{-1}$ yr^{-1} for spallation of Ti (Fink *et al.*, 2000), 1.9 ± 0.2 atoms ^{36}Cl (g Fe)$^{-1}$ yr^{-1} for spallation of Fe (Stone *et al.*, 1996), and 696 ± 185 neutrons (g air)$^{-1}$ yr^{-1} for the production rate of epithermal neutrons from fast neutrons in the atmosphere at the land/atmosphere interface (Marrero *et al.*, 2016a). A high-energy neutron attenuation length of 160 g cm^{-2} was used.

As the values of several ^{36}Cl production rates are still under discussion, most importantly the one for spallation of Ca (Schimmelpfennig *et al.*, 2011, Marrero *et al.*, 2016a), we also calculated the exposure ages using the calculator by Marrero *et al.* (2016b), which incorporates default production rates

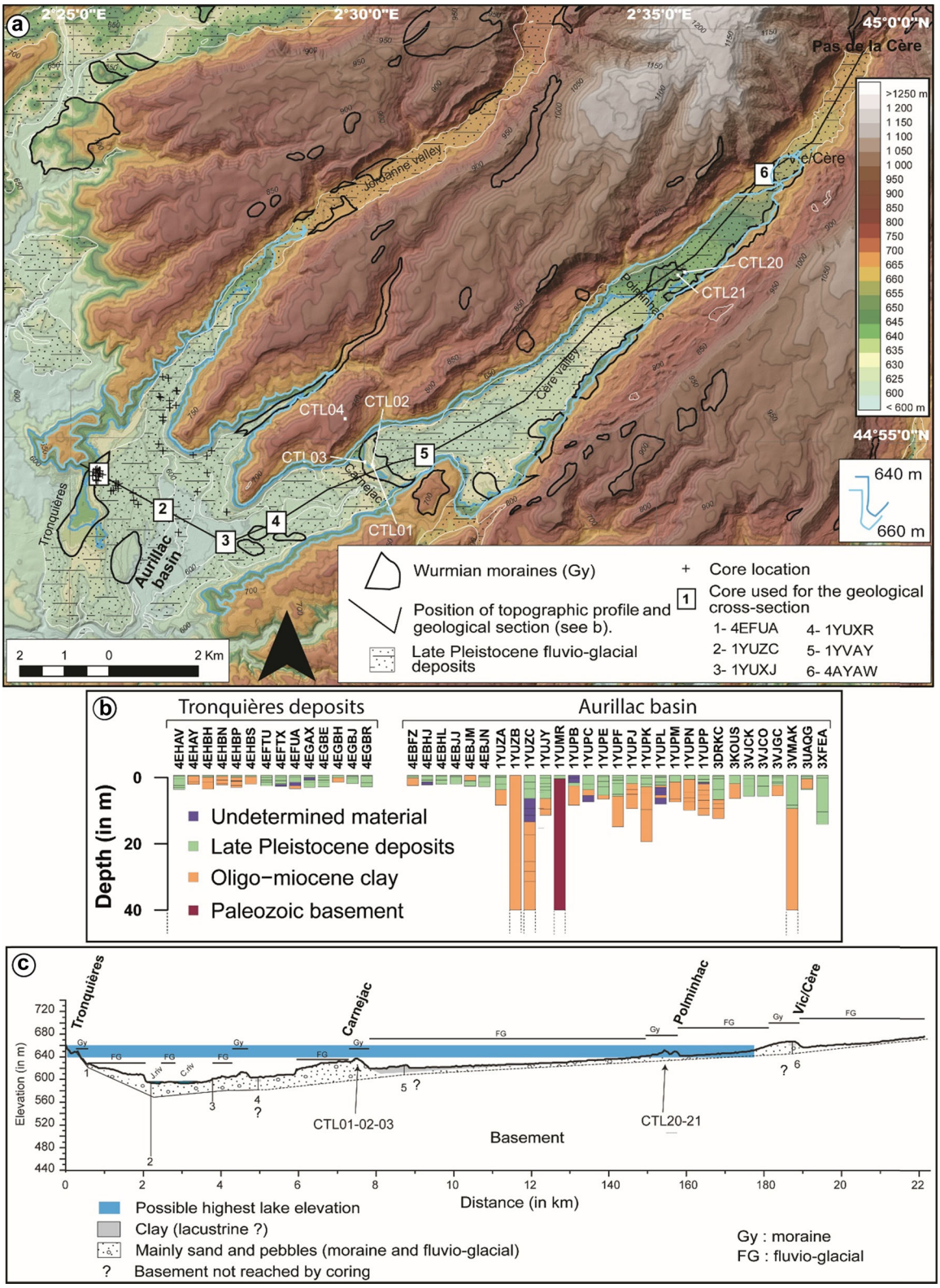

Figure 2. (a). Map of glacial and associated deposits in the lower Cère Valley, between the Pas de la Cère and the Aurillac basin, according to the 1:50 000 geological survey map (Brousse *et al.*, 1972) and location of geological cores (data available at http://infoterre.brgm.fr). (b). Interpretation of geological cores from the Tronquières moraine and the Aurillac basin. (c). Interpreted geological cross-section of the lower Cère Valley, using a geological survey map (1:50 000) and the most developed geological cores. [Color figure can be viewed at wileyonlinelibrary.com]

based on Marrero *et al.* (2016a) and the time-variant ('Lm') rather than the time-invariant ('St') scaling method used in the Excel spreadsheet of Schimmelpfennig *et al.* (2009). Due to the variations in the sample compositions and thus target element concentrations (Table 3), this leads to ages being between 0.3 ka younger and 0.2 ka older than when applying the above-described methods. These differences do not affect our chronological reconstructions.

Typical values for the erosion rates of crystalline rocks are between 0.5 and 2.5 mm.ka^{-1} in alpine environments (Balco, 2011) with a suggested value of 2 mm.ka^{-1} at mid-latitude for homogeneous rocks (André, 2002). Our sampled surfaces come

Figure 3. Photographs of erratic boulders sampled for ^{36}Cl surface exposure dating. Fractures of the CTL-01 boulder are highlighted with white dashed lines. [Color figure can be viewed at wileyonlinelibrary.com]

Table 1. Characteristics of boulders for ^{36}Cl surface exposure dating.

Sample ID	Latitude	Longitude	Elevation	Boulder lithology	Sample density	Shielding factor	Sample thickness
	(°N)	(°E)	(m a.s.l.)		(g cm^{-3})		(cm)
CTL-01	44.9108	2.5019	639	basalt	3.0	1	2.0
CTL-02	44.9112	2.5014	646	breccia	2.6	1	3.5
CTL-03	44.9111	2.4984	640	breccia	2.6	1	2.6
CTL-04	44.9200	2.4945	818	breccia	2.6	1	1.1
CTL-20	44.9503	2.5897	649	breccia	2.6	0.9985	4.6
CTL-21	44.9509	2.5913	648	basalt	3.0	0.9985	5.9

from volcanic breccia boulders (CTL-02, -03, -04, -20) composed of diverse volcanic clasts embedded in a fissile matrix (Figs. 3B–3E). Erosion processes through physical or chemical weathering are expected to be efficient and conducive to higher erosion rates than for homogeneous crystalline rocks. For example, on Gran Canaria, exposure ages and erosion rates obtained from basaltic clasts embedded in volcanic breccias were calculated using ^{3}He (Williams *et al.*, 2005). Results ranged from 2.7 to 23.9 mm.ka^{-1} for exposure ages between 25.6 and 226.2 ka. We applied three different erosion rates to our ^{36}Cl surface exposure ages: 0, 10 and 20 mm.ka^{-1} to quantified effects of various erosion rates.

Reconstruction of former glacier geometry, associated ELA and palaeoclimatic conditions

3D glacier reconstruction and ELA estimation

The geometry of the former Cère glacier was modelled in 3D using the GlaRe ArcToolBox for ArcGIS (Pellitero *et al.*, 2016) for

Table 2. Bulk composition of samples before chemical treatment, analysed at the SARM-CRPG (Nancy, France) by ICP-OES (major elements), ICP-MS (trace element), atomic absorption (Li), colorimetry (B) and spectrophotometry (Cl). Values in italics are averages from samples CTL-02, -03 for sample CTL-04.

Sample ID	SiO_2 %	Al_2O_3 %	Fe_2O_3 %	MnO %	MgO %	CaO %	Na_2O %	K_2O %	TiO_2 %	P_2O_5 %	LOI %	Total Cl (ppm)	Li (ppm)	B (ppm)	Sm (ppm)	Gd (ppm)	Th (ppm)	U (ppm)
CTL-01	53.8	18.3	8.3	0.2	1.1	5.4	4.6	3.4	1.7	0.7	2.3	125	19.4	5.1	10.6	7.9	10.8	3.0
CTL-02	51.4	15.9	9.4	0.1	2.6	6.6	2.9	2.2	2.3	0.7	6.3	285	18.5	5.0	10.4	8.4	9.1	2.6
CTL-03	51.1	17.8	9.1	0.2	2.1	7.2	3.8	2.8	2.1	0.6	2.5	98	13.9	5.2	9.2	7.2	8.5	2.3
CTL-04	*51.2*	*16.9*	*9.3*	*0.1*	*2.3*	*6.9*	*3.3*	*2.5*	*2.2*	*0.6*	*4.4*	*192*	*16.2*	*5.1*	*9.8*	*7.8*	*8.8*	*2.4*
CTL-20	53.9	15.6	7.2	0.2	4.8	5.6	4.8	3.6	1.5	0.4	1.9	225	18.8	6.5	6.6	5.4	17.1	5.0
CTL-21	43.2	13.3	12.2	0.2	10.9	10.5	3.5	1.5	2.9	0.7	1.1	760	6.4	2.3	8.1	6.7	6.9	1.7

Table 3. Concentrations in major element (in %) and in Cl (in ppm) in sample splits after acid etching, analysed at the SARM-CRPG (Nancy, France) by ICP-OES.

Sample ID	SiO_2 %	Al_2O_3 %	Fe_2O_3 %	MnO %	MgO %	CaO %	Na_2O %	K_2O %	TiO_2 %	P_2O_5 %	LOI %	Total Cl (ppm)
CTL-01	59.39	18.69	5.27	0.06	0.63	3.79	5.25	4.14	1.72	<L.D.	0.89	99.81
CTL-02	56.75	16.41	6.03	0.09	2.83	7.65	3.41	2.63	2.27	0.16	1.47	99.69
CTL-03	55.20	15.60	9.24	0.11	2.70	6.28	3.86	3.41	2.90	<L.D.	0.45	99.75
CTL-04	58.50	16.01	6.24	0.09	2.18	6.12	3.55	3.42	2.27	0.14	1.80	100.30
CTL-20	57.13	17.78	5.02	0.08	2.60	8.75	3.20	2.18	1.43	0.15	2.15	268.53
CTL-21	56.36	19.23	4.20	0.06	1.84	7.71	3.89	2.56	1.68	0.20	1.76	98.74

the three glacial stadials recognised in the field (Fig. 4). This model assumes a perfect plasticity behaviour for glacier ice and applies the numerical iterative solution to the Van der Veen's equation (Benn and Hulton, 2010). The basal shear stress value generally lies between 50 kPa and 150 kPa (Benn and Evans, 2010). The appropriate basal shear stress value was estimated to match the reconstructed ice thickness according to geomorphological markers on the valley sides, i.e. lateral moraines. Ice-thickness profiles were reconstructed along 70 flowlines that were manually digitised along the main glacial valley trunk and its network tributaries. Glacier surface was interpolated using the *Topo to Raster* method to produce a 100×100 m cell-size resolution DEM of the former glacier surface topography. A valley-shape correction factor (f) of 0.7 (average f value obtained from 79 valley cross-sections) was applied to account for the valley morphology effect.

Palaeo-ELAs were estimated using the ELA Calculation ToolBox for ArcGIS (Pellitero *et al.*, 2015) and the area–altitude balance ratio method. Different balance ratio values were associated with different glacier/climate relationships and a range of 1.0–2.5 with 0.5 intervals was applied to consider the global balance ratio value reported in Rea (2009). The mean with its standard deviation was then reported for each glacial stadial.

The Cère Valley topography was affected by landslides, especially deep-seated landslides. The topography of the palaeo-glacier bed has an influence on the 3D glacier modelling and the ELA estimation (Pellitero *et al.*, 2016, 2015). In the absence of a robust chronology for the landslides, glacier modelling was run with both the post-landslide topography (i.e. the current topography) and the pre-landslide topography. The pre-landslide topography was reconstructed following the methodology given in Rodríguez-Rodríguez *et al.* (2018).

Palaeoclimatic reconstructions

As no glaciers are currently present in the Massif Central, a direct comparison between the current ELA and former ELAs was impossible. In order to estimate the amplitude of ELA changes and to quantify the effect of oceanic influences that control the Cantal climate (Jubertie, 2006), the current theoretical ELA was assessed using current climatic conditions derived from 21 climatic stations located in western Cantal (Figs. 1 and 4A). Climatic conditions were extrapolated to higher altitude using a linear regression and plotted against the Ohmura equation (Fig. 4C) which provides a relationship between the mean summer temperature (MST in °C) and the mean annual precipitation (MAP in mm yr^{-1}) at the ELA (derived from an inventory of 70 glaciers in the world; Ohmura *et al.*, 1992). By graphic read out, the intersection between the extrapolated current climatic conditions above summits of the Cantal Mounts and the Ohmura equation yielded an MST of 7.6 ± 0.3°C and an MAP of 3162 ± 163 mm yr^{-1}. These climatic conditions were converted to elevation in metres, using current altitudinal lapse rates of 840 mm $yr^{-1}.km^{-1}$ and 5.0°C.km^{-1} (Fig. 4A). A similar lapse rate for MST has been reconstructed reflecting the potential effects of dominant southwestern influences in the Cère Valley (Valadas, 1984) to 5.5°C.km^{-1} (Genevois *et al.*, 2022). This yielded a current theoretical ELA at 2759 ± 28 m (Fig. 4C). A higher altitudinal lapse rate for MST (i.e. 5.5°C km^{-1}) decreased the current theoretical ELA to 2634 m a.s.l. Once the ELA was calculated for current climatic conditions and for former glacial stadials, MST values were calculated according to a −90% to 0% change of MAP compared with present, using the Ohmura equation (Ohmura *et al.*, 1992) and current climatic gradients. This assumption did not account for palaeo-climatic gradients prevailing during the LGM and the Last Glacial-to-Interglacial Transition (LGIT) in Europe (Heyman *et al.*, 2013; Peyron *et al.*, 1998).

Mean July temperature (MJT) data reconstructed from chironomid assemblages of the Oldest Dryas and the YD at the Roustières sites were used to estimate theoretical MAP at the ELA (Figs. 1 and 4). These data indicate an MJT of 6–10°C for the Oldest Dryas and 10–13°C for the YD. These two periods are drier than today according to pollinic assemblages (Gandouin *et al.*, 2016; Ponel *et al.*, 2016). First, palaeo-MJTs were converted into MSTs using the current linear relationships (0.98 factor; Fig. 4B). Then the summer cooling was estimated by comparing palaeo-MSTs with current MSTs recorded by local climatic stations. This cooling was applied to the current climate

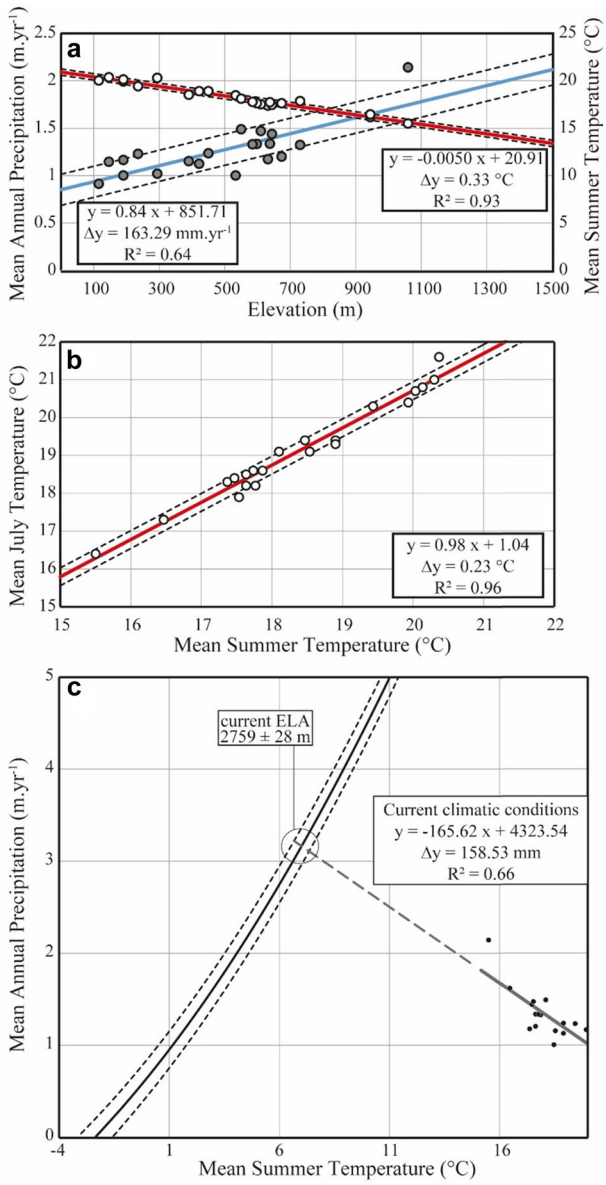

Figure 4. Climatic conditions in the western Cantal Mounts. (a). Mean summer temperature (MST) and mean annual precipitation (MAP) from the 21 climatic stations, plotted against elevation and associated elevation gradients. Black dots are mean annual precipitation. White dots are mean annual temperatures. (b). Linear regression of mean July temperature (MJT) against MST. (c). Calculated current theoretical equilibrium line altitude from interpolation of the 21 climatic stations against the Ohmura equation. [Color figure can be viewed at wileyonlinelibrary.com]

in the Cère Valley to obtain theoretical MSTs during the period of interest. No correction for altitude was performed as the Roustières site altitude frame reconstructed ELAs for the Carnéjac and the Polminhac stadials. The Ohmura equation was used to calculate the associated MAP. As the Roustières elevation (1196 m a.s.l.) approximates the ELA reconstruction elevations for the Carnéjac and the Polminhac stadials, no elevation correction was performed on the calculated MSTs and MAP.

Results

Glacial geomorphology

No significant glacial deposits were found in the upper part of the Cère Valley. Here, multiple head valleys with amphitheatre morphologies have developed in trachyandesitic rocks (Fig. 5A). These topographic settings were associated with limited ice accumulation, except for the Fond d'Alagnon glacial cirque in the Alagnon Valley which ice contributed to the Cère Valley glacier by a glacier transfluence towards the Fond de Cère pass (1290 m) (Fig. 5A). In contrast, in the lower part of the Cère Valley, large glacial landforms constituting a specific landform assemblage, such as moraines and proglacial outwash were found, particularly in the Aurillac basin (Fig. 6). Geomorphological observations enabled a partial reconstruction of the deglaciation sequence despite disturbances caused by slope deposits (alluvial fans, colluvial accumulation and landslides) or fluvial processes (incision and aggradation of the valley floor) which may have masked, reworked or buried glacial landforms and the associated deposits (Fig. 6).

All glacial and associated deposits identified in this work were located between the Tronquières moraine and the Pas de la Cère. The Tronquières moraine in the Aurillac basin (644 m a.s.l.; Figs. 2 and 6) reveals the maximal extent of the Cère glacier. According to geological cores (Fig. 2), these deposits are composed of diamicton 2–4 m thick, interpreted as till of undetermined age. Three levels of terrace above the current Cère river +10, +20, +30 m (Figs. 2 and 6)—were identified on the eastern slope of the Tronquières moraine, at the Cère and the Jordanne rivers' confluence. Around 5.5 km upstream of the Tronquières moraine, the Carnéjac end moraine (640 m a.s.l.) forms a transverse topographic ridge in the Cère Valley. This landform was associated with fluvio-glacial deposits forming a 3 km long perched (+15 to +5 m) terrace above the current Cère River. Near the proximal Carnéjac end-moraine slope, clayey sediments were reported (Figs. 2 and 6), interpreted as potential lacustrine deposits. The Polminhac end moraine (650 m a.s.l.), located 14 km upstream of the Tronquières moraine, is constituted of two individual, smooth and parallel ridges across the valley (Fig. 2). An alluvial cone partly masked this end moraine. On the Cère Valley slopes, the La Pradelle lateral moraine (925 m a.s.l.) was identified (Figs. 6 and 7) and is associated with the Carnéjac stadial. In addition, isolated patches of till and isolated erratic boulders were found at the Vézac pass (665 m a.s.l.), at the Puy des Arbres pass (880 m a.s.l.) and at the Curebourse pass (1000 m a.s.l.). These glacial deposits attest to tansfluences of the Cère glacier towards secondary valleys (Fig. 6). The Vic-sur-Cère landform is interpreted as an alluvial fan in relation to a marked gully. These glacial landforms allow the definition of at least three glacier stadials. The Tronquières stadial for which the Tronquières moraine gives a minimal extent. As no new observations were performed, the earlier assumption that associated these deposits with pre-LLGM glacial advance was not modified (Veyret, 1978). However, tills were identified between the Troquières moraine and the Carnéjac end moraine. Based on their fresh aspects, i.e. no weathering traces, these deposits are associated with the LLGM. The Carnéjac and the Polminhac stadials were associated with two glacier standstills during the deglaciation.

Between the Carnéjac end moraine and the Pas de la Cère, large landslides affected the valley slopes. The largest one was the Vixouze landslide in which till deposits filled longitudinal gullies that were subsequently moulded by subglacial erosion (Figs. 5C, 5E, 6 and 7). These observations suggest that the Vixouze landslide, and by extension other smaller landslides in the Cère Valley, occurred before the Carnéjac stadial.

Chronological results

All samples have $^{36}Cl/^{35}Cl$ ratios in the range of $8.9–14.8 \times 10^{-14}$ compared with two process blanks (BKCTL-01 and −02) with

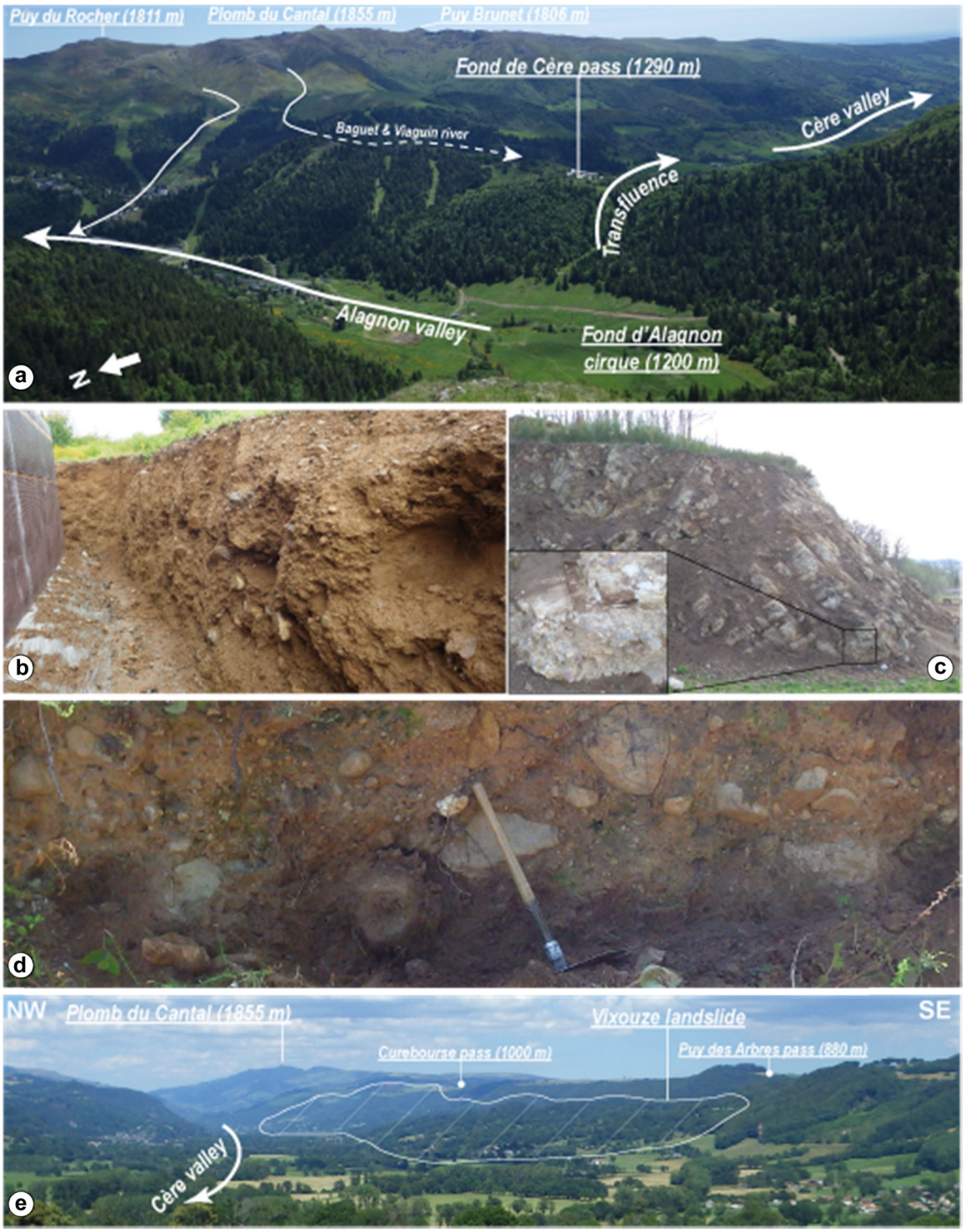

Figure 5. Photographs of geomorphological features in the Cère Valley. (a). The Fond d'Alagnon glacial cirque and the Alagnon glacier transfluence towards the Cère Valley. (b). Basal till deposits (Local Last Glacial Maximum, LLGM) at the Vézac pass. (c). Fossilised alluvion under basaltic table in the Vixouze landslide constituting slide masses. (d). Ice-marginal deposits (LLGM) forming terraces at the Vézac pass. (e). View of the lower Cère Valley, showing the extent of the Vixouze landslide. [Color figure can be viewed at wileyonlinelibrary.com]

$^{36}Cl/^{35}Cl$ ratios of 2.32 ± 0.6 and $0.12 \pm 0.04 \times 10^{-15}$, respectively. Typical uncertainties for raw AMS data are 1.7–3.0% for $^{35}Cl/^{37}Cl$ and 6.2–9.3% for $^{36}Cl/^{35}Cl$. Measurement results, calculated concentrations and surface exposure ages with their uncertainties are reported in Table 4.

For samples CTL-01 and CTL-03, the correction of surface exposure ages with a 10 and a 20 mm.ka^{-1} erosion rate led to older ages (Table 4; Fig. 8). In these samples, Cl concentrations are low (~30 ppm; Table 4). All other samples (CTL-02, -04, -20 and -21) give younger exposure ages when applying 10 and 20 mm.ka^{-1} erosion rates (Fig. 8). This is counter-intuitive when correcting exposure ages for erosion but these samples have high Cl concentrations (between ~99 and 521 ppm; Table 4). This high Cl concentration induces higher ^{36}Cl concentration in the subsurface than at the surface through low-energy-neutron capture by ^{35}Cl.

Surface exposure ages corrected with a 10 mm.ka^{-1} erosion rate were assumed to best reflect boulders' erosion since their exposure. The stratigraphically oldest erratic boulder (CTL-04) is isolated and located on the Cavanhac plateau and has an exposure age of 13.5 ± 3.9 ka (Table 4). This sample was taken from an erratic boulder associated with the LLGM retreat,

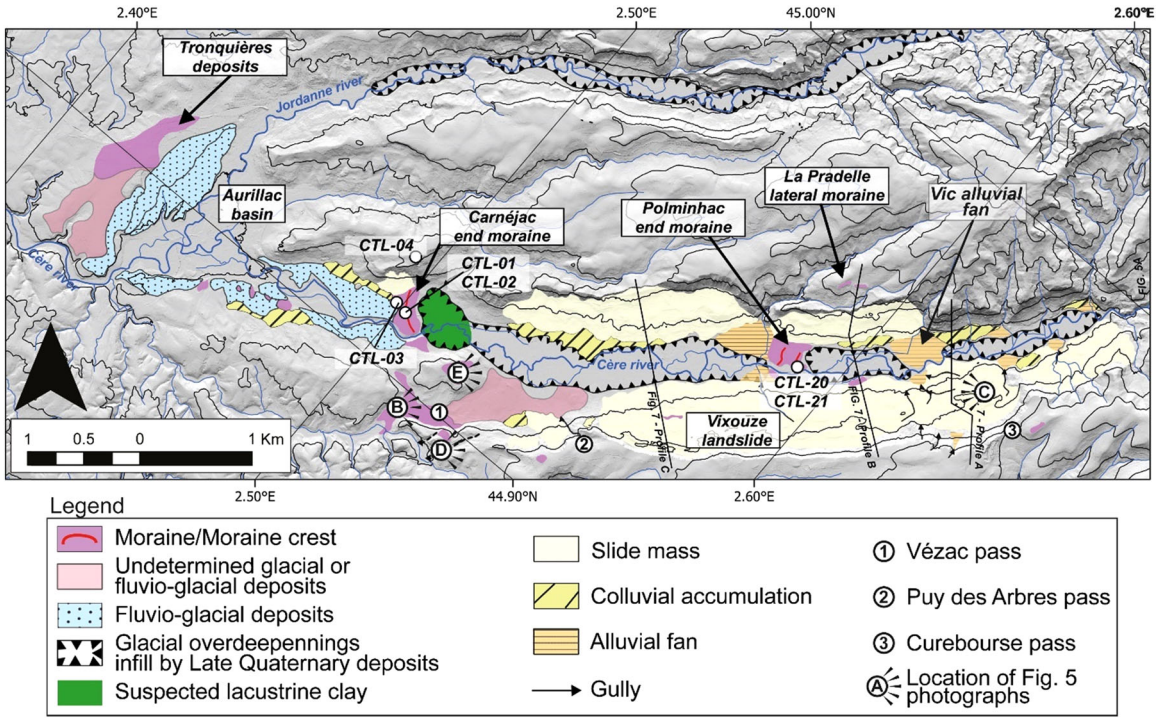

Figure 6. Map of glacial and slope deposits and location of the ^{36}Cl samples in the lower part of the Cère Valley. [Color figure can be viewed at wileyonlinelibrary.com]

before the Carnéjac stadial (Figs. 3D, 6 and 8). Three moraine boulders embedded in the Carnéjac end moraine were sampled (Table 4; Figs. 3A–3C, 6 and 8). Sample CTL-01 was taken from a basaltic boulder characterised by fractures and jigsaw cracks (Fig. 6A). Samples CTL-02 and CTL-03 were taken from volcanic breccia boulders (Figs. 3B and 3C). Surface exposure ages are clustered: 12.6 ± 1.2 ka (CTL-01), 12.0 ± 2.2 ka (CTL-02) and 12.2 ± 1.1 ka (CTL-03), whereby only CTL-02 was a Cl-rich sample. Two volcanic breccia boulders were sampled from the inner ridge of the Polminhac end moraine (Figs. 3E–3F, 6 and 8): CTL-20 (Cl-rich sample) yielded a maximum exposure age of 12.1 ± 2.6 ka and CTL-21 an exposure age of 0.9 ± 0.3 ka. Due to its position near the Cère River (~40 m) and its small size (~0.2 m^3 above ground), the CTL-21 boulder is interpreted as an exhumed boulder associated with probable later fluvial or anthropogenic end-moraine erosion.

We note that ^{36}Cl surface exposure ages from two distant (~8 km apart) end moraines: the Carnéjac and the Polminhac moraines, are well clustered to ~12 ka ($n = 4$; Fig. 8). The interpretation of these ages is discussed in 'Interpretation and discussion' section.

Glacier modelling

We performed 3D reconstructions of the palaeo-Cère glacier with the position of Carnéjac and Polminhac end moraines. We extended the glacier flowline to the Font d'Alagnon glacial cirque to take into account the glacier transfluence at this place (Fig. 5A). The elevation of the La Pradelle lateral moraine (Figs. 6 and 7B) indicate a palaeo-ice thickness of 280 m, compatible with a basal shear stress of 25 kPa for the lower part of the Cère valley during the Carnéjac stadial. However, typical values of basal shear stress for valley glaciers were 50–150 kPa (Benn and Evans, 2010). Our low value for basal shear stress supports rapid basal sliding compatible with deformable sediments at the glacier bed. Such deformable sediments could be represented by Oligocene and Miocene uncemented clayey sediments or Late Pleistocene deposits, which composed the lower Cère Valley floor (Figs. 2 and 6). For the uppermost half of the valley a basal shear stress value of 100 kPa was used. We note that the topography of the glacier bed changed before and after the landslides. However, the two distinct topographic configurations did not significantly affect the reconstructed palaeo-glaciers and associated ELAs. An ELA of 1078 ± 43 m a.s.l. for a pre-landslide topography and an ELA of 1091 ± 43 m a.s.l. for a post-landslide topography was calculated (Table 5). Because we found till, associated with the Carnéjac stadial, in transversal gullies of the Vixouze landslide (Figs. 6 and 7C): (i) we hypothesise that the age of the majority of landslides in the Cère Valley are associated with pre-Carnéjac stadial periods; and (ii) we chose the post-landslide topography to reconstruct the Carnéjac and the Polminhac stadials. The glacier modelling of the Polminhac stadial was processed using the same basal shear stress values as for the Carnéjac stadial. Only the main flowline was adjusted to match the respective end moraine.

During the Carnéjac stadial, only the Curebourse pass was reached by the palaeo-glacier that potentially flowed over into the Goul Valley (Figs. 6 and 7). The other two transfluences identified in the field were probably active during the LLGM or at times when more ice accumulated in the valley. Reconstructed ELAs for the Carnéjac stadial (1091 ± 43 m a.s.l.) and for the Polminhac stadial (1152 ± 34 m a.s.l.) are indistinguishable within uncertainties (Table 5). These ELA values were comparable to those reconstructed in Western Europe for the LGM (see Kuhlemann *et al.*, 2008 for a synthesis).

Based on the MJTs for the Oldest Dryas and the YD from the Roustières site, the associated MJTs at the ELA were calculated and are summarised in Table 5. Results indicate a 9.2–5.4°C cooling for the Oldest Dryas with a +141 to +230% MAP at the ELA and a 5.4 to 2.6°C cooling for the YD with a +230 to +305% MAP at the ELA compared with today (Table 5). During these two periods, the reconstructed MAP gives a wetter climate than today, which is not consistent with local and regional palaeoenvironmental data. This discrepancy is partially due to the temperature not being cold enough to calculate the MAP at the ELAs. The

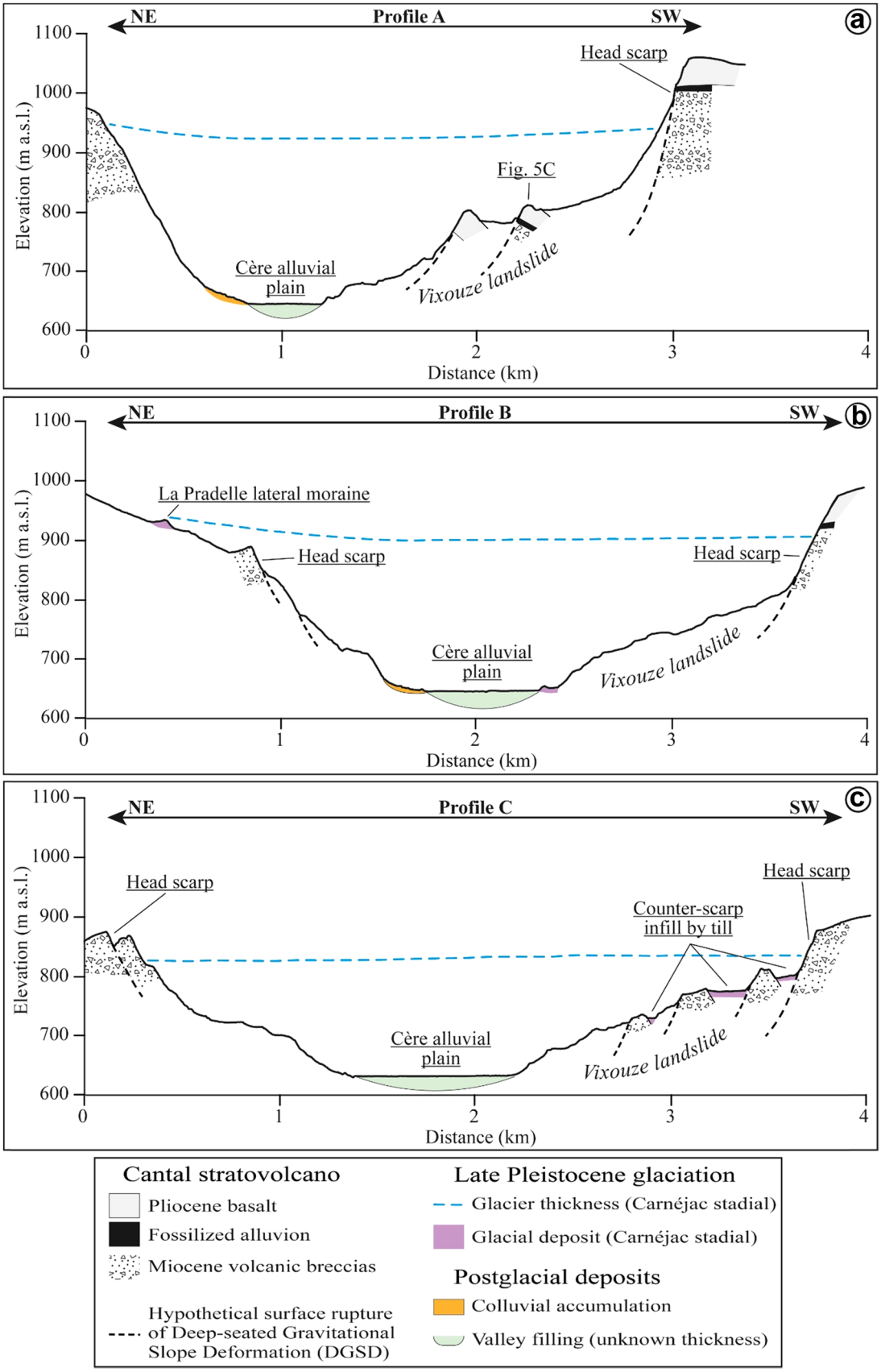

Figure 7. Transverse profiles of the lower Cère Valley showing relationships between deep-seated gravitational slope deformations and the former glacier. (a). Transversal profile located upstream from the Vic alluvial fan. (b). Transversal profile located upstream from the Polminhac end moraine. (c). Transversal profile located upstream from the Carnéjac end moraine. For precise location of profiles see Figure 6. [Color figure can be viewed at wileyonlinelibrary.com]

Table 4. Relevant data for chemical ^{36}Cl extraction, AMS results and ^{36}Cl exposure ages.

Sample ID	Sample weight (g)	Mass of Cl in spike (mg)	$[^{35}Cl/^{37}Cl]$	$[^{36}Cl/^{35}Cl]$ (10^{-14})	Number of atoms Cl (10^{19})	[Cl] in sample (ppm)	$[^{36}Cl]$ (10^6 atoms)	$[^{36}Cl]$ (10^4 at.g^{-1})	Age (ka)* including p uncertainties $\varepsilon = 0$ mm yr^{-1}	Age (ka)* including p uncertainties $\varepsilon = 10$ mm yr^{-1}	Age (ka)* including p uncertainties $\varepsilon = 20$ mm yr^{-1}
Plateau de Cavanhac											
CTL-04**	43.59	1.8117	3.459 ± 0.059	11.1 ± 0.8	38.60 ± 7.03	521 ± 95	35.80 ± 6.42	82.14 ± 14.73	16.9 ± 3.9 (4.9)	13.5 ± 3.9 (4.9)	13.3 ± 3.9 (4.9)
Moraine de Carnéjac											
CTL-01	42.97	1.8020	8.703 ± 0.150	14.8 ± 0.9	2.25 ± 0.13	31 ± 2	7.07 ± 0.48	16.44 ± 1.11	12.0 ± 1.2 (1.3)	12.6 ± 1.2 (1.3)	13.9 ± 1.2 (1.3)
CTL-02**	44.09	1.8020	3.757 ± 0.067	9.5 ± 0.7	20.20 ± 2.34	270 ± 31	17.38 ± 2.10	39.42 ± 4.76	13.6 ± 2.2 (3.0)	12.0 ± 2.2 (3.0)	12.1 ± 2.2 (3.0)
CTL-03	40.41	1.8096	8.684 ± 0.262	13.7 ± 0.8	2.27 ± 0.16	33 ± 2	6.57 ± 0.44	16.26 ± 1.09	11.8 ± 1.1 (1.3)	12.2 ± 1.1 (1.3)	13.2 ± 1.1 (1.3)
Moraine de Polminhac											
CTL-20	45.07	2.0010	3.807 ± 0.115	8.9 ± 0.5	20.56 ± 3.60	269 ± 47	17.01 ± 2.65	3.78 ± 0.59	13.6 ± 2.6 (2.6)	12.1 ± 2.6 (2.6)	12.3 ± 2.6 (2.6)
CTL-21**	45.15	1.9998	4.961 ± 0.149	1.8 ± 0.2	7.57 ± 0.72	99 ± 9	1.64 ± 0.18	0.36 ± 0.04	0.96 ± 0.3 (0.3)	0.9 ± 0.3 (0.3)	0.9 ± 0.3 (0.3)
BKCTL-01	-	1.7632	376.034 ± 9.772	0.23 ± 0.06	-	-	-	-	-	-	-
BKCTL-02	-	1.9914	212.416 ± 8.504	0.012 ± 0.004	-	-	-	-	-	-	-

*No snow correction.
**Cl-rich sample.

Figure 8. Camel plots of ^{36}Cl exposure ages under different erosion rate scenarios (black line: 0 mm.ka^{-1}, green line: 10 mm.ka^{-1}, red line: 20 mm.ka^{-1}) against local glacial chronologies and the chronological scenario of postglacial evolution of the Cère Valley. Camel plots were generated using the Matlab code from G. Balco (https://cosmognosis.wordpress.com/2009/07/13/matlab-code-for-camel-diagrams/). a) Glacial chronology of the Aubrac lateau icefield from ^{10}Be and ^{26}Al exposure ages (Ancrenaz *et al.*, 2022). b) Relative glacial chronology established by Veyret (1978) for the CCMD last glaciation. c) Relative glacial chronology established by Etlicher and Goër de Hervé (1988) for the CCMD last glaciation. 1: Local Last Glacial Maximum, 2: Minor glacier advance, 3: Cirque glacier stade, A: Glacier retreat, B: Full deglaciation. d) Schematic representation of the sediment yield during the paraglacial period (modified from Ballantyne, 2002) against our chronological scenario for ;the deglaciation, the postglacial and the 'modern' periods. The convergence of ^{36}Cl exposure ages (green box) is interpreted as the end of the paraglacial period and the beginning of the 'modern' period (see text for more details). [Color figure can be viewed at wileyonlinelibrary.com]

source of this incompatibility is discussed in the following section.

Interpretation and discussion

^{36}Cl surface exposure ages interpretation: boulder exhumation related to a postglacial event?

^{36}Cl surface exposure ages obtained in the Cère Valley range between 13 and 11 ka (Table 4) and are coeval with the YD ($n = 3$ for the Carnéjac end moraine and $n = 1$ for the Polminhac end moraine). Sample CTL-04 from the stratigraphically oldest boulder gives an older surface exposure age with a broad uncertainty (Table 4; Fig. 8). This exposure age could reflect a minimum age for the LLGM end but it is not further discussed here as it is a single dated erratic boulder.

Table 5. Synthesis of Carnéjac and Polminhac equilibrium line altitude (ELA) reconstructions and associated climatic conditions using local mean July temperature (MJT) for the Younger Dryas and the Oldest Dryas.

				Roustières site (1196 m a.s.l.)			
		Current climatic conditions at ELA altitude		Younger Dryas climatic conditions at ELA		Oldest Dryas climatic conditions at ELA	
	ELA (m)	MST (°C)	MAP ($mm.yr^{-1}$)	MST (°C)	MAP anomaly (%)	MST (°C)	MAP anomaly (%)
Carnéjac stade (post-landslide topography)	1091 ± 43	15.5 ± 0.2	1771 ± 36	9.5–12.4	+230 – +305	5.7–9.5	+141–+230
Carnéjac stade (pre-landslide topography)	1078 ± 43	15.5 ± 0.2	1760 ± 37				
Polminhac stade	1152 ± 34	15.2 ± 0.2	1823 ± 29				
Today	2759 ± 28	7 ± 1	3162 ± 159	-	-	-	-

MAP: mean annual precipitation; MST: mean summer temperature.

The association of the Carnéjac or the Polminhac end moraines with the YD cold event is not plausible considering:

- the existing relative and local chronologies for the CCMD glacier fluctuations (Veyret, 1978; Etlicher and Goër de Hervé, 1988). These early chronological hypotheses are supported by local palaeoenvironmental data and surface exposure ages (^{10}Be and ^{26}Al) from the nearby Aubrac Mounts (Ancrenaz *et al.*, 2022). Both palaeoenvironmental and exposure ages support a deglaciation of the CCMD at the end of the Oldest Dryas (Fig. 8). During the YD, either only cirque glaciers occurred in the CCMD, according to Veyret (1978), or the CCMD was fully deglaciated, according to Etlicher and Goër de Hervé (1988).
- the ELAs and associated palaeoclimatic conditions reconstructed for these two stadials in the Cère Valley (between 1078 ± 43 and 1152 ± 34 m; Table 5), which are comparable to reconstructions from the Alps or the Pyrenees during the LGM or the early LGIT (Ivy-Ochs *et al.*, 2008; Kuhlemann *et al.*, 2008; Reixach *et al.*, 2021).

Two explanations for this apparent time lag between the expected glacial chronology of the CCMD and the ^{36}Cl surface exposure ages obtained in the Cère Valley (this study) are considered. First, existing relative glacial chronologies for the CCMD underestimate the intensity of glacial advances during the YD. This means that associated climatic conditions in the CCMD were colder than expected to sustain these two major glacier stadials. Nevertheless, local palaeoenvironmental data converge towards robust reconstructions of the YD in the CCMD (Juvigné *et al.*, 1996; Miras *et al.*, 2006; Miras and Guenet, 2013; Ponel *et al.*, 1991; Vergne, 1991) and are not consistent with our mapped glacier advances.

The second hypothesis relies on uncertainties regarding the geomorphological events leading to the exhumation of the sampled boulders. Indeed, boulders embedded in end moraines could record incomplete exposure histories (Heyman *et al.*, 2011) induced by geomorphological evolution of the end moraine. Two processes could lead to underestimated surface exposure ages: erosion of the sampled surfaces and incomplete exposure. The effects of erosion on the sampled surface were quantified by correcting surface exposure ages for various erosion rates and results show comparable ages (Table 4; Fig. 8). Generally, incomplete exposure is regarded as the main liming effect in the use of surface exposure ages (Heyman *et al.*, 2011). Incomplete exposure encompasses the effects of post-depositional burial or exhumation that led to underestimated surface exposure ages. For example, end-moraine slope destabilisation after the deglaciation is considered to be one of the main processes leading to incomplete exposure of boulders, by boulder rolling, burial or latter exhumation through erosional processes (Allard *et al.*, 2020; Heyman *et al.*, 2011; Putkonen and Swanson, 2003; Tomkins *et al.*, 2021; Zreda *et al.*, 1994).

In the Cère Valley, ^{36}Cl surface exposure ages obtained for the Carnéjac end moraine and the Polminhac end moraine were: (i) interpreted as non-related glacial events; and (ii) constrained between 13 and 11 ka. We argue that these boulders experienced the same incomplete exposure history with a first phase of burial with shielding and then a simultaneous exhumation related to a unique and rapid geomorphological event concerning both the Carnéjac and the Polminhac end moraines. This geomorphological event took place after the deglaciation of the Cère Valley. This hypothesis is further developed in the following section.

Geomorphological scenarios for the postglacial evolution of the Cère Valley

Geomorphological observations concerning the postglacial evolution of the lower Cère Valley, between the Aurillac basin and the Pas de la Cère (Fig. 2 for location), are summarised here:

- Intensive geomorphological activities on valley slopes such as gullies incision, alluvial fans (Vic fan; Fig. 6), shallow landslides and colluvial accumulation.
- The valley floor is composed of up to 15–20 m of Pleistocene sediments, i.e. till, fluvio-glacial, fluvial or slope deposits, according to geological cores (Fig. 2).
- Three terrace levels were identified in the Aurillac basin (+10, +20 and +30 m; Fig. 6).
- Between the Carnéjac end moraine and the Pas de la Cère, two flat topographic levels on the valley floor are reported at 640 m—related to the Carnéjac end moraine—and at 660 m —related to the Polminhac end moraine.
- Finally, clayey deposits against the proximal slopes of the Carnéjac end moraines were identified and were interpreted as lacustrine clay from a moraine-dammed proglacial lake by Veyret (1978).

The resulting landform-sediment assemblage is interpreted as a typical paraglacial landscape (Ballantyne, 2002). The Cère Valley filling is related to the hydro-sediment are continuity perturbation during postglacial evolution, inducing intensive aggradation dynamics between the Carnéjac end moraine and the Pas de la Cère. Intense slope activities due to paraglacial conditions is enhanced by the overall lithologies of the Cère

Valley tributaries (heterogenous volcanic breccias and trachytic rocks) favourable to glacial debuttressing, landsliding and fluvial erosion, which support a perturbated hydro-sedimentary continuity by enhanced sediment supply in the Cère Valley.

To explain the synchronous ^{36}Cl surface exposure ages from the Carnéjac ($n = 3$) and the Polminhac ($n = 1$) end moraines separated by 8 km, we combined our (i) literature review, (ii) geological core compilation and (iii) fieldwork, to propose two complementary geomorphological scenarios: the Aurillac proglacial lake and the postglacial Cère River fluvial incision. The two scenarios encompass potential evolutions of the Cère Valley leading to boulder burial. These scenarios rely on two major assumptions: the Carnéjac and the Polminhac stadials were coeval to glacier-favourable periods identified in the Aubrac Mounts between 25 and 17 ka and the Cère Valley deglaciation is coeval with the Aubrac Mounts deglaciation ~17 ka (Ancrenaz *et al.* 2022). In addition, the potential effects of anthropogenic disturbance (agricultural activities and urbanization) were not accounted for in these scenarios.

The Aurillac proglacial lake scenario

The Tronquières moraine (644 m a.s.l.) is assumed to be LLGM deposits. During the Cère glacier retreat the Tronquières moraine could have dammed the valley, enclosing the Aurillac basin and producing a moraine-dammed proglacial lake: the Aurillac Lake (Fig. 9). The lake surface altitude reached between 640 and 660 m a.s.l. (deepest part between ~50 and ~70 m in the Aurillac basin), was 18 km long at its maximum with a total surface area ranging between 32 and 44 km^2. The following Carnéjac and Polmihnac stadials and their associated end moraines were deposited in a glaciolacustrine environment (Fig. 9). The Aurillac Lake shielded, at least partially, boulders from the Carnéjac and the Polminhac end moraines from cosmic rays. At some point during deglaciation, the Tronquières moraine was breached by the Cère River, lowering the Aurillac proglacial lake level and exposing the boulders. Carnéjac and Polminhac end moraines dammed the valley, producing secondary lakes that did not shield end-moraine crests and the sampled boulders. As the Tronquières moraine was breached, fluvial terraces in the Aurillac basin were constructed while minor lakes subsisted in the valley (Fig. 9). In this scenario, ^{36}Cl surface exposure ages from the Carnéjac and the Polminhac boulders (13–11 ka) are considered to be the maximum ages for their exhumation and correspond to the timing of the Aurillac Lake drainage.

Postglacial fluvial incision scenario

After the LLGM, the Cère Valley glacier retreated and the Carnéjac and the Polminhac stadials occurred during deglaciation. As no moraine-dammed lakes were present in the Aurillac basin, the Carnéjac and the Polminhac end moraines were deposited in a terrestrial ice-marginal environment. The construction of alluvial terraces in the Aurillac basin were coeval with the Cère Valley deglaciation. After the full deglaciation, the Carnéjac and the Polminhac end moraines produced moraine-dammed lakes associated with aggradation dynamics by lacustrine sedimentation on the valley floor. These dynamics are enhanced by intense slope activities. During this period of aggradation, end moraines were stable landforms and sampled boulders were buried and fully shielded by at minimum 4 m of till. The end of aggradation dynamics was associated to a change in the hydro-sedimentary dynamics, leading to the Cère River fluvial incision of end moraines. This erosional phase was responsible for the end moraine destabilisation leading to boulder exhumation. In this scenario, ^{36}Cl surface exposure ages (13–11 ka) reflected the end moraines' stabilisation after an intensive erosional phase associated with the end of postglacial aggradation dynamics.

Each of these two scenarios have limitations. For the Aurillac proglacial lake scenario, the true age of the Tronquières moraine is still uncertain. However, the identification of fresh aspect tills in the Aurillac basin associated with the LLGM (this study) offset the pre-LLGM hypothesis from Veyret (1978). In addition, no lacustrine deposits were identified with certainty in the Aurillac basin. For the postglacial fluvial incision scenario, the well-preserved topography of the Carnéjac and the Polminhac end moraines was the main limitation, which indicated limited post-deposition erosion of these landforms. Furthermore, the important size of the sampled boulders (Fig. 3) favoured limited effects of postglacial exhumation through end-moraine erosion (Heyman *et al.*, 2016).

Despite these limitations, our two scenarios highlight the wide range of postglacial geomorphological events that could have affected the lower Cère Valley morphology and then could have impacted the ^{36}Cl surface exposure ages of the boulders. The true postglacial evolution is probably a combination of the two geomorphological scenarios: moraine-dam lake breaching and consecutive fluvial incision. More precisely, it is highly probable that proglacial lakes between the Carnéjac and the Polminhac end moraines have subsisted for a longer time than the lake between Aurillac and Carnéjac (Fig. 9). This is suggested by the distinct evolution between the Aurillac basin, affected by a longer fluvial incision (three terrace levels for nearly 30 m of vertical incision), compared with the Carnéjac–Polminhac–Pas de la Cère area, where no fluvial terraces are observed (a very limited incision of 10 m at the Carnéjac moraine).

The chronological signal recorded by our ^{36}Cl ages, between 13 and 11 ka, occurred 5 ka after the deglaciation and records an abrupt change in the hydor-sediment continuity in the Cère Valley. We interpret the chronological signal as an exhumation age of the sampled boulders, due to the end of aggradation dynamics and the beginning of fluvial incision that demarcated the end of the postglacial evolution of the Cère Valley (Figs. 8 and 9). By comparison, in deglaciated valleys of the Alps, the postglacial valley-filling duration was estimated to be up to 7 ka (Brardinoni *et al.*, 2018), which is consistent with our scenarios. The end of the valley-filling is mainly controlled by the timing of the tributaries' deglaciation, slope stabilisation and climatic conditions (Brardinoni *et al.*, 2018; Ravazzi *et al.*, 2012). A combination of all three factors was expected to control the end of the postglacial adjustment in the Cère Valley (13–11 ka).

Conclusions

The Cère Valley was occupied by a glacier during the last glaciation and sediment assemblages provided an opportunity to reconstruct glacial fluctuations in the CCMD. Revision of geomorphological arguments allows us to identify three glacial stadials. The Tronquières moraine marks the last maximal extent of the glacier but it was not possible to identify whether it was deposited by a pre-LLGM glacier advance or an LLGM glacier advance. As a working hypothesis we attributed the glacial deposits in the Aurillac basin to the LLGM. Two other glacier stadials, the Carnéjac and the Polminhac stadials, are defined by end moraines that indicate two major glacial events. Large landslides in the Cère Valley pre-dated these two glacier stadials (based on the presence of till in landslide counter-slopes). ^{36}Cl surface exposure ages from one erratic boulder, three boulders embedded in the Carnéjac end moraine and two boulders embedded in the Polminhac end

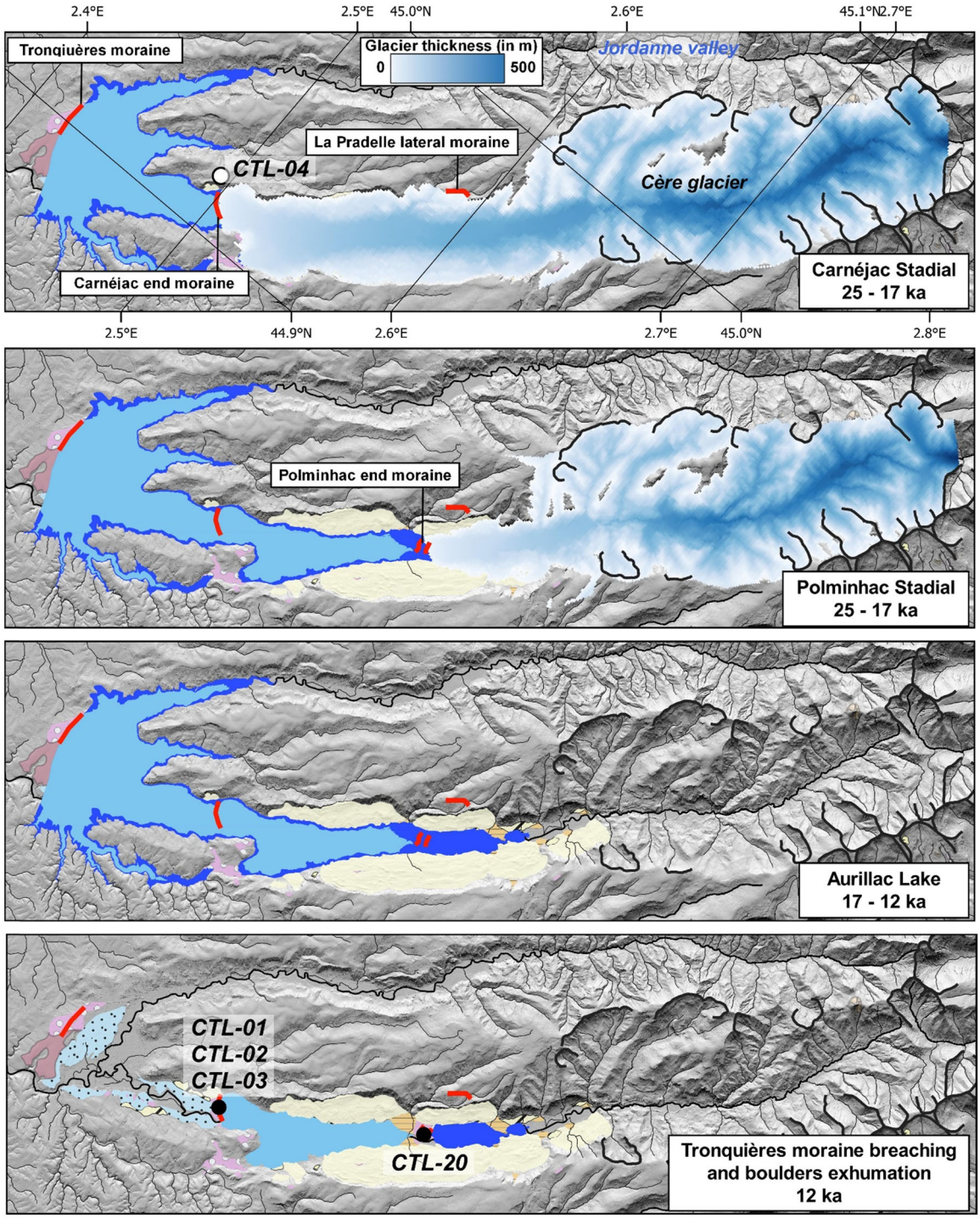

Figure 9. Reconstruction of the last deglaciation in the Cère Valley according to the Aurillac proglacial lake scenario. Two lake levels were represented: 640 m in light blue and 660 m in dark blue. Black lines delineated glacial cirques. For the legend see Fig. 6. [Color figure can be viewed at wileyonlinelibrary.com]

moraine were obtained. Results are coeval to the YD and range between 13 and 11 ka. The ages are too young considering the hypothesised ages of these end moraines according to existing relative glacial chronologies in the CCMD and the direct glacial chronology from the nearby Aubrac Mounts. Moreover, 3D reconstructions and associated ELAs with prevailing climatic conditions (MST and MAP) calculated for the Carnéjac and the Polminhac stadials are comparable to those calculated for the LGM and the early LGIT in the Alps and the Pyrenees.

To explain the time lag between ^{36}Cl surface exposure ages and expected end-moraine ages, we investigated geomorphological scenarios that could have led to a later exhumation of the sampled boulders. Using geomorphic observations, geological cores and ^{36}Cl surface exposure ages, two scenarios were presented: the Aurillac proglacial lake scenario and the postglacial fluvial incision scenario. Each scenario explains plausible causes of boulder burial and then exhumation by one unique geomorphological event. The geomorphological scenario judged as the more plausible indicated that after the Cère Valley glaciation, between 25 and 17 ka, moraine-dammed lakes and intensive slope activities under paraglacial conditions led to the Cère Valley filling. During this period, the Carnjéac and the Polminhac end moraines were stable landforms with sampled boulders buried and shielded from cosmic rays. This postglacial evolution (>17 to ~12 ka) was

ended by the Cère River fluvial incision, eroding the base of the end moraines which lowered their surfaces and exposed the sampled boulders (~12 ka). However, future geomorphological investigations in the CCMD are needed to validate and complete this scenario.

This work shows that our ^{36}Cl surface exposure ages are related to a major geomorphological event at the Cère Valley scale, during its postglacial evolution. Those geomorphological processes need to be fully understood and are complementary to direct chronologies and 3D glacier reconstructions to correctly reconstruct glacial fluctuations. In other formerly glaciated Cantal valleys, such as the Alagnon Valley, the same landform assemblage is identified (a flat valley floor filled by Pleistocene sediments). This highlights the potential complex postglacial evolution of several Cantal valleys that is still poorly known and for which this work provides a few first-order hypotheses.

Acknowledgments and funding. The authors thank Mr Christophe Ribes and Mr Jean-Marie Lafon, inhabitants of Carnéjac, for giving us permission to access erratic boulders located on their properties. ^{36}Cl analyses were performed at the ASTER AMS national facility (CEREGE, Aix-en-Provence), supported by the INSU/CNRS, by the ANR through the 'Projets thématiques d'excellence' programme for the 'Equipements d'excellence' ASTER-CEREGE action, and by the Institut de Recherche pour le Développement (IRD). This project was co-funded by INSU-SYSTER and was partially funded by the Ice-Collapse project (the dynamics of ice sheet collapse in deglaciation periods) supported by the French Agence Nationale de la Recherche through grant ANR-18-CE01-0009.

Data availability atatement

Data available on request from the authors.

References

Allard JL, Hughes PD, Woodward JC. 2021. Heinrich Stadial aridity forced Mediterranean-wide glacier retreat in the last cold stage. *Nat. Geosci.* **14**: 197–205. https://doi.org/10.1038/s41561-021-00703-6

Allard JL, Hughes PD, Woodward JC, Fink D, Simon K, Wilcken KM. 2020. Late Pleistocene glaciers in Greece: a new 36Cl chronology. *Quaternary Science Reviews* **245**: 106528. https://doi.org/10.1016/j.quascirev.2020.106528

Ancrenaz A, Define E, Poiraud A. 2020. Fluctuations glaciaires au Pléistocène supérieur dans les Monts d'Aubrac (Massif central, France): nouvelles données. *Géomorphologie: relief, processus, environnement* **26**: 16. https://doi.org/10.4000/geomorphologie.14516

Ancrenaz A, Braucher R, Define E, Poiraud A, Steiger J. 2022. Last glacial fluctuations in the southwestern Massif Central, Aubrac (France): First direct chronology from cosmogenic ^{10}Be and ^{26}Al exposure dating. *Quaternary Science Reviews* **285**: 107500. https://doi.org/10.1016/j.quascirev.2022.107500

André M-F. 2002. Geomorphic evidence for recurrent cold-based ice conditions in Nordic uplands during the Quaternary glaciations (Aurivaara Plateau, North Sweden). *Norsk Geografisk Tidsskrift - Norwegian Journal of Geography* **56**: 74–79. https://doi.org/10.1080/002919502760056387

Arnaud N, Leyrit H, Nehlig P, Binet F, Jamet A, Vannier W. 2002. Lahars on the north-western flank of the Cantal stratovolcan 11.

Arnold M, Aumaître G, Bourlès DL, Keddadouche K, Braucher R, Finkel RC, Nottoli E, Benedetti L, Merchel S. 2013. The French accelerator mass spectrometry facility ASTER after 4years: Status and recent developments on ^{36}Cl and ^{129}I. *Nuclear Instruments and Methods in Physics Research Section B: Beam Interactions with Materials and Atoms* **294**: 24–28. https://doi.org/10.1016/j.nimb.2012.01.049

Balco G. 2011. Contributions and unrealized potential contributions of cosmogenic-nuclide exposure dating to glacier chronology, 1990–2010. *Quaternary Science Reviews* **30**: 3–27. https://doi.org/10.1016/j.quascirev.2010.11.003

Balco G, Stone JO, Lifton NA, Dunai TJ. 2008. A complete and easily accessible means of calculating surface exposure ages or erosion rates from ^{10}Be and ^{26}Al measurements. *Quaternary Geochronology, Prospects for the New Frontiers of earth and Environmental Sciences* **3**: 174–195. https://doi.org/10.1016/j.quageo.2007.12.001

Ballantyne CK. 2002. Paraglacial geomorphology. Quaternary Science Reviews 83.

Benn DI, Evans DJA. 2010. *Glaciers and Glaciation*. Second Edition. ed. Hodder Education: London.

Benn DI, Hulton NRJ. 2010. An ExcelTM spreadsheet program for reconstructing the surface profile of former mountain glaciers and ice caps. *Computers & Geosciences* **36**: 605–610. https://doi.org/10.1016/j.cageo.2009.09.016

Blaauw M. 2010. Methods and code for 'classical' age-modelling of radiocarbon sequences. *Quaternary Geochronology* **5**: 512–518. https://doi.org/10.1016/j.quageo.2010.01.002

Boisse de Black Y. 1951. Les glaciations de l'Auvergne: massif du Cantal, Cézallier, Monts-Dore, étude géographique et géologique. impr. Moderne, Aurillac.

Borchers B, Marrero S, Balco G, Caffee M, Goehring B, Lifton N, Nishiizumi K, Phillips F, Schaefer J, Stone J. 2016. Geological calibration of spallation production rates in the CRONUS-Earth project. *Quaternary Geochronology* **31**: 188–198. https://doi.org/10.1016/j.quageo.2015.01.009

Boule M. 1896. La topographie glaciaire en Auvergne. *Annales de Géographie* **5**: 277–296. https://doi.org/10.3406/geo.1896.6883

Boule M. 1895. Les glaciers pliocènes et quaternaires de l'Auvergne. *Comptes rendus hebdomadaires des séances de l'Académie des Sciences* **121**: 837–839.

Brardinoni F, Picotti V, Maraio S, Bruno PP, Cucato M, Morelli C, Mair V. 2018. Postglacial evolution of a formerly glaciated valley: Reconstructing sediment supply, fan building, and confluence effects at the millennial time scale. *GSA Bulletin* **130**: 1457–1473. https://doi.org/10.1130/B31924.1

Calvet M, Delmas M, Gunnell Y, Braucher R, Bourlès D. 2011. Recent Advances in Research on Quaternary Glaciations in the Pyrenees, in: *Developments in Quaternary Sciences*. Elsevier, 127–139. https://doi.org/10.1016/B978-0-444-53447-7.00011-8.

Degeai J-P, Pastre J-F. 2009. Impacts environnementaux sur l'érosion des sols au Pléistocène supérieur et à L'holocène dans le cratère de maar du lac du Bouchet (Massif central, France). *Quaternaire* **20**(2): 149–159. https://doi.org/10.4000/quaternaire.5101

Define E, Raynal JP, Ancrenaz A, Poiraud A. 2019. L'englacement quaternaire du Massif central, in: Histoire de la découverte géologique du Massif central français, Mémoire. Société d'Histoire Naturelle d'Auvergne, p. 267.

Delmas M, Calvet M, Gunnell Y, Braucher R, Bourlès D. 2011. Palaeogeography and ^{10}Be exposure-age chronology of Middle and Late Pleistocene glacier systems in the northern Pyrenees: Implications for reconstructing regional palaeoclimates. *Palaeogeography, Palaeoclimatology, Palaeoecology* **305**: 109–122. https://doi.org/10.1016/j.palaeo.2011.02.025

Ehlers J, Gibbard PL, Hughes PD. 2011. Quaternary Glaciations - Extent and Chronology, Elsevier. ed, Developments in Quaternary Science.

Etlicher B, Goër de Hervé A(de). 1988. La déglaciation würmienne dans le Massif Central français, le point des travaux récents/The Würmian déglaciation in the French Massif-Central, review of recent works. *Bulletin de l'Association française pour l'étude du quaternaire* **25**: 103–110. https://doi.org/10.3406/quate.1988.1871

Fink D, Vogt S, Hotchkis M. 2000. Cross-sections for 36Cl from Ti at Ep=35–150 MeV: Applications to in-situ exposure dating. *Nuclear Instruments and Methods in Physics Research Section B: Beam Interactions with Materials and Atoms* **172**: 861–866. https://doi.org/10.1016/S0168-583X(00)00200-7

Gandouin E, Rioual P, Pailles C, Brooks SJ, Ponel P, Guiter F, Djamali M, Andrieu-Ponel V, Birks HJB, Leydet M, Belkacem D, Haas JN, Van der Putten N., de Beaulieu JL. 2016. Environmental and climate reconstruction of the late-glacial-Holocene transition from a lake sediment sequence in Aubrac, French Massif Central: Chironomid and diatom evidence. *Palaeogeography, Palaeoclimatology, Palaeoecology* **461**: 292–309. https://doi.org/10.1016/j.palaeo.2016.08.039

Genevois V, Martin C, Morel J-M, Poiraud A, Suc O, Laveuf C, Vautier A, Decugis E, Marcou P, Foret M, Rahimian V. 2022. Référenciel Régional Pédologique du Cantal, étude n°30150.

Glangeaud P. 1921. Essai de synthèse sur les anciens glaciers du Massif central. *Compte rendu sommaire Société Géologique de France* **4ème série, tome XXI**: 119.

Goër de Hervé A(de). 1972. La Planèze de Saint-Flour: structure et géomorphologie glaciaire. Univ. Clermont II.

Heyman BM, Heyman J, Fickert T, Harbor JM. 2013. Paleo-climate of the central European uplands during the last glacial maximum based on glacier mass-balance modeling. *Quat. res.* **79**: 49–54. https://doi.org/10.1016/j.yqres.2012.09.005

Heyman J, Applegate PJ, Blomdin R, Gribenski N, Harbor JM, Stroeven AP. 2016. Boulder height – exposure age relationships from a global glacial ^{10}Be compilation. *Quaternary Geochronology* **34**: 1–11. https://doi.org/10.1016/j.quageo.2016.03.002

Heyman J, Stroeven AP, Harbor JM, Caffee MW. 2011. Too young or too old: Evaluating cosmogenic exposure dating based on an analysis of compiled boulder exposure ages. *Earth and Planetary Science Letters* **302**: 71–80. https://doi.org/10.1016/j.epsl.2010.11.040

Hughes PD, Gibbard PL. 2015. A stratigraphical basis for the Last Glacial Maximum (LGM. *Quaternary International* **383**: 174–185. https://doi.org/10.1016/j.quaint.2014.06.006

Ivy-Ochs S, Kerschner H, Reuther A, Preusser F, Heine K, Maisch M, Kubik PW, Schlüchter C. 2008. Chronology of the last glacial cycle in the European Alps. *J. Quaternary Sci* **23**: 559–573. https://doi.org/10.1002/jqs.1202

Jubertie F. 2006. Les excès climatiques dans le Massif central français. L'impact des temps forts pluviométriques et anémométriques en Auvergne. Université Blaise Pascal - Clermont Ferrand II.

Julien A, Laval E. 1868. Sur l'existence d'anciens glaciers dans le Puy-de-Dôme et le Cantal, et sur l'origine véritable des conglomérats ponceux de la colline de Perrier. *Comptes rendus hebdomadaires des séances de l'Académie des Sciences* **67**: 1356–1357.

Juvigné E, Bastin B, Delibrias G, Evin J, Gewelt M, Gilot E, Streel M. 1996. A comprehensive pollen- and tephra-based chronostratigraphic model for the Late Glacial and Holocene period in the French Massif Central. *Quaternary International* **34–36**: 113–120. https://doi.org/10.1016/1040-6182(95)00075-5

Kleman J, Borgström I. 1996. RECONSTRUCTION OF PALAEO-Ice SHEETS: THE USE OF GEOMORPHOLOGICAL DATA. *Earth Surface Processes and Landforms* **21**: 893–909. https://doi.org/10.1002/(SICI)1096-9837(199610)21:10%3C893::AID-ESP620%3E3.0.CO;2-U

Kuhlemann J, Rohling EJ, Krumrei I, Kubik P, Ivy-Ochs S, Kucera M. 2008. Regional Synthesis of Mediterranean Atmospheric Circulation During the Last Glacial Maximum. *Science* **321**: 1338–1340. https://doi.org/10.1126/science.1157638

Leibrandt S. 2011. Reconstitution de l'évolution morpho-structurale et de la dynamique éruptive du massif du Cantal: relation avec la distribution spatio-temporelle du volcanisme du Massif Central (France). Univ. Paris Sud 2.

Marrero SM, Phillips FM, Borchers B, Lifton N, Aumer R, Balco G. 2016a. Cosmogenic nuclide systematics and the CRONUScalc program. *Quaternary Geochronology* **31**: 160–187. https://doi.org/10.1016/j.quageo.2015.09.005

Marrero SM, Phillips FM, Caffee MW, Gosse JC. 2016b. CRONUS-Earth cosmogenic ^{36}Cl calibration. *Quaternary Geochronology* **31**: 199–219. https://doi.org/10.1016/j.quageo.2015.10.002

Merchel S, Bremser W, Alfimov V, Arnold M, Aumaître G, Benedetti L, Bourlès DL, Caffee M, Fifield LK, Finkel RC, Freeman SPHT, Martschini M, Matsushi Y, Rood DH, Sasa K, Steier P, Takahashi T, Tamari M, Tims SG, Tosaki Y, Wilcken KM, Xu S. 2011. Ultra-trace analysis of ^{36}Cl by accelerator mass spectrometry: an interlaboratory study. *Anal Bioanal Chem* **400**: 3125–3132. https://doi.org/10.1007/s00216-011-4979-2

Miras Y, Guenet P. 2013. Une histoire plurimillénaire des paysages du Cézallier et ses liens avec les activités agrosylvo- pastorales depuis le Néolithique à partir de l'analyse pollinique de la tourbière de La Borie (1170 m, Saint-Saturnin, Cantal) 17.

Miras Y, Surmely F, Guenet P, Vannière B, Walter-Simonnet A-V. 2006. Dynamiques d'occupation et histoire de l'environnement d'un terroir de moyenne montagne: la tourbière de Peyre (Lacapelle-Barrès, Cantal, Massif central) et ses alentours. *Presses Universitaires de Franche-Compté* **799**: 157.

Murton JB, Ballantyne CK. 2017. Chapter 5 Periglacial and permafrost ground models for Great Britain. *EGSP* **28**: 501–597. https://doi.org/10.1144/EGSP28.5

Nehlig P, Leyrit H, Dardon A, Freour G, de Goër A, Huguet D, Thieblemont D. 2001. Constructions et destructions du stratovolcan du Cantal. *Bulletin de la Société Géologique de France* **172**: 295–308.

Ohmura A, Kasser P, Funk M. 1992. Climate at the equilibrium line of glaciers. *Journal of Glaciology* **38**: 397–411.

Pellitero R, Rea BR, Spagnolo M, Bakke J, Hughes P, Ivy-Ochs S, Lukas S, Ribolini A. 2015. A GIS tool for automatic calculation of glacier equilibrium-line altitudes. *Computers & Geosciences* **82**: 55–62. https://doi.org/10.1016/j.cageo.2015.05.005

Pellitero R, Rea BR, Spagnolo M, Bakke J, Ivy-Ochs S, Frew CR, Hughes P, Ribolini A, Lukas S, Renssen H. 2016. GlaRe, a GIS tool to reconstruct the 3D surface of palaeoglaciers. *Computers & Geosciences* **94**: 77–85. https://doi.org/10.1016/j.cageo.2016.06.008

Peyron O, Guiot J, Cheddadi R, Tarasov P, Reille M, de Beaulieu J-L, Bottema S, Andrieu V. 1998. Climatic Reconstruction in Europe for 18,000 YR B.P. from Pollen Data. *Quaternary Research* **49**: 183–196. https://doi.org/10.1006/qres.1997.1961

Ponel P, Etlicher B, De Beaulieu JL, Debard E, Thinon M, Vasari A, Petiot R. 1991. La fin de la dernière glaciation dans le Cantal (France): la tourbière de La Taphanel et son environnement. *Quaternaire* **2**: 147–163. https://doi.org/10.3406/quate.1991.1964

Ponel P, Guiter F, Gandouin E, Pailles C, Rioual P, Djamali M, Andrieu-Ponel V, Leydet M, Van der Putten N, de Beaulieu J-L. 2016. Novel insights from coleopteran and pollen evidence into the Lateglacial/Holocene transition in Aubrac, French Massif Central. *Palaeogeography, Palaeoclimatology, Palaeoecology* **463**: 83–102. https://doi.org/10.1016/j.palaeo.2016.09.020

Ponel P, Russell Coope G. 1990. Lateglacial and Early Flandrian Coleoptera from La Taphanel, Massif Central, France: Climatic and Ecological Implications. *Journal of Quaternary Science* **5**: 235–249. https://doi.org/10.1002/jqs.3390050306

Putkonen J, Swanson T. 2003. Accuracy of cosmogenic ages for moraines. *Quaternary Research* **59**: 255–261. https://doi.org/10.1016/S0033-5894(03)00006-1

Rames J-B. 1873. Géogénie du Cantal avec une étude historique et critique sur les progrès des la géologie dans ce département. 116.

Ravazzi C, Badino F, Marsetti D, Patera G, Reimer PJ. 2012. Glacial to paraglacial history and forest recovery in the Oglio glacier system (Italian Alps) between 26 and 15 ka cal bp. *Quaternary Science Reviews* **58**: 146–161. https://doi.org/10.1016/j.quascirev.2012.10.017

Rea BR. 2009. Defining modern day Area-Altitude Balance Ratios (AABRs) and their use in glacier-climate reconstructions. *Quaternary Science Reviews* **28**: 237–248. https://doi.org/10.1016/j.quascirev.2008.10.011

Reille M, Beaulieu J-L(de). 1988. History of the Würm and Holocene vegetation in western Velay (Massif Central, France): a comparison of pollen analysis from three corings at Lac du Bouchet. *Review of Palaeobotany and Palynology* **54**: 233–248.

Reimer PJ, Austin WEN, Bard E, Bayliss A, Blackwell PG, Bronk Ramsey C, Butzin M, Cheng H, Edwards RL, Friedrich M, Grootes PM, Guilderson TP, Hajdas I, Heaton TJ, Hogg AG, Hughen KA, Kromer B, Manning SW, Muscheler R, Palmer JG, Pearson C, van der Plicht J, Reimer RW, Richards DA, Scott EM, Southon JR, Turney CSM, Wacker L, Adolphi F, Büntgen U, Capano M, Fahrni SM, Fogtmann-Schulz A, Friedrich R, Köhler P, Kudsk S, Miyake F, Olsen J, Reinig F, Sakamoto M, Sookdeo A, Talamo S. 2020. The IntCal20 Northern Hemisphere Radiocarbon Age Calibration Curve (0–55 cal kbp. *Radiocarbon* **62**: 725–757. https://doi.org/10.1017/RDC.2020.41

Reixach T, Delmas M, Braucher R, Gunnell Y, Mahé C, Calvet M. 2021. Climatic conditions between 19 and 12 ka in the eastern Pyrenees, and wider implications for atmospheric circulation patterns in Europe. *Quaternary Science Reviews* **260**: 106923. https://doi.org/10.1016/j.quascirev.2021.106923

Rodríguez-Rodríguez L, González-Lemos S, Ballesteros D, Valenzuela P, Domínguez-Cuesta MJ, Llana-Fúnez S, Jiménez-Sánchez M. 2018. Timing of paraglacial rock-slope failures and denudation signatures in the Cantabrian Mountains (North Iberian Peninsula. *Land Degrad Dev* **29**: 3159–3173. https://doi.org/10.1002/ldr.3012

Schimmelpfennig I, Benedetti L, Finkel R, Pik R, Blard P-H, Bourlès D, Burnard P, Williams A. 2009. Sources of in-situ 36Cl in basaltic rocks. Implications for calibration of production rates. *Quaternary Geochronology* **4**: 441–461. https://doi.org/10.1016/j.quageo.2009.06.003

Schimmelpfennig I, Benedetti L, Garreta V, Pik R, Blard P-H, Burnard P, Bourlès D, Finkel R, Ammon K, Dunai T. 2011. Calibration of cosmogenic 36Cl production rates from Ca and K spallation in lava flows from Mt. Etna (38°N, Italy) and Payun Matru (36°S, Argentina). *Geochimica et Cosmochimica Acta* **75**: 2611–2632. https://doi.org/10.1016/j.gca.2011.02.013

Schimmelpfennig I, Schaefer JM, Putnam AE, Koffman T, Benedetti L, Ivy-Ochs S, Team A, Schlüchter C. 2014. 36 Cl production rate from K-spallation in the European Alps (Chironico landslide, Switzerland): 36 Cl PRODUCTION RATE AND K-SPALLATION. *J. Quaternary Sci.* **29**: 407–413. https://doi.org/10.1002/jqs.2720

Stone JO. 2000. Air pressure and cosmogenic isotope production. *Journal of Geophysical Research* **105**: 753–759.

Stone JO, Allan GL, Fifield LK, Cresswell RG. 1996. Cosmogenic chlorine-36 from calcium spallation. *Geochimica et Cosmochimica Acta* **60**: 679–692. https://doi.org/10.1016/0016-7037(95)00429-7

Tomkins MD, Dortch JM, Hughes PD, Huck JJ, Pallàs R, Rodés Á, Allard JL, Stimson AG, Bourlès D, Rinterknecht V, Jomelli V, Rodríguez-Rodríguez L, Copons R, Barr ID, Darvill CM, Bishop T. 2021. Moraine crest or slope: An analysis of the effects of boulder position on cosmogenic exposure age. *Earth and Planetary Science Letters* **570**: 117092. https://doi.org/10.1016/j.epsl.2021.117092

Valadas B. 1984. Les hautes terres du Massif central français: contribution à l'étude des morphodynamiques récentes sur versants cristallins et volcaniques. Univ. Panthéon-Sorbonne (Paris I).

Van Dorsser HJ. 1986. La vallée du Brezon et les plateaux adjaçents. *Revue de Géomorphologie Dynamique* **35**: 113–121.

Van Dorsser HJ. 1982. Carte géomorphologique du Sud-Ouest du Massif du Cantal. *Revue de Géomorphologie Dynamique* **31**: 1–35.

Vergne V. 1991. Les paysages végétaux d'Artense au Tardiglaciaire et à l'Holocène (Vegetal landscapes in the Artense region during Late-glacial and Holocene). *Bulletin de l'Association de Géographes Français* **68**: 23–28. https://doi.org/10.3406/bagf.1991.1555

Veyret Y. 1978. Les modelés et formations d'origine glaciaire dans le Massif central français: problèmes de distribution et de limites dans un milieu de moyenne montagne. Univ. Panthéon-Sorbonne (Paris I).

Veyret-Mekdjian Y, Brousse P, Delibrias G. 1978. Première datation d'un épisode glaciaire récent dans le Massif central français. *Comptes rendus hebdomadaires des séances de l'Académie des Sciences* **286**: 1089–1092.

Williams AJ, Stuart FM, Day SJ, Phillips WM. 2005. Using pyroxene microphenocrysts to determine cosmogenic ^{3}He concentrations in old volcanic rocks: an example of landscape development in central Gran Canaria. *Quaternary Science Reviews* **24**: 211–222. https://doi.org/10.1016/j.quascirev.2004.07.004

Wirsig C, Zasadni J, Christl M, Akçar N, Ivy-Ochs S. 2016. Dating the onset of LGM ice surface lowering in the High Alps. *Quaternary Science Reviews* **143**: 37–50. https://doi.org/10.1016/j.quascirev.2016.05.001

Zreda MG, Phillips FM, Elmore D. 1994. Cosmogenic ^{36}Cl accumulation in unstable landforms: 2. Simulations and measurements on eroding moraines. *Water Resources Research* **30**: 3127–3136. https://doi.org/10.1029/94WR00760